Proteomic identification of novel cytoskeletal proteins associated with TbPLK, an essential regulator of cell morphogenesis in *Trypanosoma brucei*

Michael R. McAllaster[a,*], Kyojiro N. Ikeda[b,*,†], Ana Lozano-Núñez[c,‡], Dorothea Anrather[d], Verena Unterwurzacher[d], Thomas Gossenreiter[d], Jenna A. Perry[a], Robbie Crickley[e], Courtney J. Mercadante[a], Sue Vaughan[e], and Christopher L. de Graffenried[a]

[a]Department of Molecular Microbiology and Immunology, Brown University, Providence, RI 02912; [b]Max F. Perutz Laboratories, Department of Medical Biochemistry, Medical University of Vienna, 1030 Vienna, Austria; [c]Max F. Perutz Laboratories, Center for Molecular Biology, University of Vienna, 1030 Vienna, Austria; [d]Max F. Perutz Laboratories, Mass Spectrometry Facility, University of Vienna, 1030 Vienna, Austria; [e]Department of Biological and Medical Sciences, Faculty of Health and Life Science, Oxford Brookes University, Oxford OX3 0BP, United Kingdom

ABSTRACT ***Trypanosoma brucei* is the causative agent of African sleeping sickness, a devastating disease endemic to sub-Saharan Africa with few effective treatment options. The parasite is highly polarized, including a single flagellum that is nucleated at the posterior of the cell and adhered along the cell surface. These features are essential and must be transmitted to the daughter cells during division. Recently we identified the *T. brucei* homologue of polo-like kinase (TbPLK) as an essential morphogenic regulator. In the present work, we conduct proteomic screens to identify potential TbPLK binding partners and substrates to better understand the molecular mechanisms of kinase function. These screens identify a cohort of proteins, most of which are completely uncharacterized, which localize to key cytoskeletal organelles involved in establishing cell morphology, including the flagella connector, flagellum attachment zone, and bilobe structure. Depletion of these proteins causes substantial changes in cell division, including mispositioning of the kinetoplast, loss of flagellar connection, and prevention of cytokinesis. The proteins identified in these screens provide the foundation for establishing the molecular networks through which TbPLK directs cell morphogenesis in *T. brucei*.**

Monitoring Editor
Stephen Doxsey
University of Massachusetts

Received: Apr 15, 2015
Revised: Jun 16, 2015
Accepted: Jun 24, 2015

This article was published online ahead of print in MBoC in Press (http://www.molbiolcell.org/cgi/doi/10.1091/mbc.E15-04-0219) on July 1, 2015.

*These authors contributed equally to this work.

Present addresses: †Sir William Dunn School of Pathology, University of Oxford, Oxford OX1 3RE, United Kingdom; ‡Department of Bioanalysis, Macherey-Nagel, 52355 Düren, Germany.

Address correspondence to: Christopher L. de Graffenried (Christopher_deGraffenried@Brown.edu).

Abbreviations used: BSF, bloodstream form; CPC, chromosomal passenger complex; FAZ, flagellum attachment zone; FC, flagella connector; FPC, flagellar pocket collar; iTRAQ, isobaric tags for relative and absolute quantitation; MtQ, microtubule quartet; PCF, procyclic form; SILAC, stable isotope labeling by amino acids in cell culture; TbPLK, *T. brucei* polo-like kinase.

INTRODUCTION

Trypanosoma brucei is the causative agent of human African trypanosomiasis in humans and nagana in cattle (Pays and Vanhollebeke, 2009; Brun *et al.*, 2010; Mott *et al.*, 2011; Welburn and Maudlin, 2012). These diseases cause tremendous harm in sub-Saharan Africa, in terms of both human health and economic stability (Fèvre *et al.*, 2008). *T. brucei* is a unicellular eukaryote that is transmitted by the bite of the *Glossina* fly and cycles between two primary forms: the insect-resident procyclic form (PCF) and the mammalian-resident bloodstream form (BSF), which are both obligate extracellular pathogens that must disseminate effectively throughout their hosts to survive (Matthews and Gull, 1994; MacGregor *et al.*, 2011; Aksoy *et al.*, 2013).

Trypanosomes are highly polarized cells that are optimized to survive constant contact with the defenses of their hosts (Gull, 1999; Langousis and Hill, 2014). A series of subpellicular microtubules

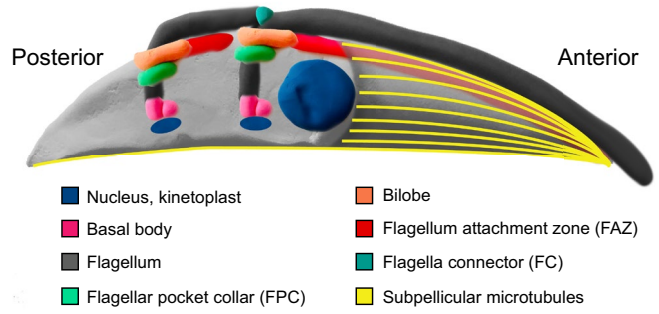

FIGURE 1: Schematic of key cellular organelles involved in flagellum positioning. Model of a cell approximately halfway through cell division, where all the key cytoskeletal structures, such as the FC, are present or have already duplicated.

underlies the cell surface, producing a cell with a long, tapered shape and distinct posterior and anterior ends (Figure 1; Sherwin and Gull, 1989; Robinson and Gull, 1991; Schneider *et al.*, 1997). A single flagellum is nucleated at the posterior end of the cell from a basal body, which is linked to the mitochondrial DNA aggregate known as the kinetoplast (Vaughan, 2010; Langousis and Hill, 2014). Depending on the life cycle stage, the kinetoplast and basal body can be positioned to the posterior of the nucleus (trypomastigote) or toward the anterior (epimastigote; Hoare and Wallace, 1966). The flagellum transits through an invagination of the cell surface known as the flagellar pocket, which is the only compartment that is competent for endocytosis and exocytosis (Gull, 2003; Field and Carrington, 2009). The flagellar pocket is tightly cinched at its top by the flagellar pocket collar (FPC), which encircles the flagellum (Bonhivers *et al.*, 2008; Lacomble *et al.*, 2009). A second cytoskeletal structure, known as the bilobe, is found to the dorsal side of the FPC and forms a hook around the flagellum (He *et al.*, 2005; Esson *et al.*, 2012).

The flagellum is adhered along the cell surface after exiting the flagellar pocket and extends for several micrometers past the anterior end of the cell. Flagellar attachment is mediated by a structure known as the flagellum attachment zone (FAZ), comprising a series of junctions that span the plasma and flagellar membranes, forming a tight seal (Figure 1; Vickerman, 1969). The FAZ also includes a set of four microtubules, known as the microtubule quartet (MtQ), which nucleate at the basal body, wrap around the flagellar pocket, and assume a position next to the filament (Gull, 1999; Lacomble *et al.*, 2009). Cell polarity and flagellar attachment are essential for the motility of the parasite, which is necessary for transmission and for evasion of the host immune system (LaCount *et al.*, 2002; Engstler *et al.*, 2007). This positional information must be transmitted to the daughter cells along with the correct complement of organelles during cell division to produce progeny that can survive within their hosts (McKean, 2003; Hammarton *et al.*, 2007b; Farr and Gull, 2012).

The process of flagellar positioning has been well described morphologically in *T. brucei* (Moreira-Leite *et al.*, 2001; Gadelha *et al.*, 2009; Lacomble *et al.*, 2009, 2010). This process begins with the maturation of the probasal body, which docks with the flagellar pocket membrane and nucleates a new flagellum (Lacomble *et al.*, 2010; André *et al.*, 2013). In PCFs, the new flagellum is physically linked to the old flagellum by a structure known as the flagella connector (FC), which is believed to direct the positioning of the new flagellum by using the old one as a template (Figure 1; Moreira-Leite *et al.*, 2001; Briggs *et al.*, 2004). The linked flagella are partitioned into separate flagellar pockets once they emerge onto the cell surface as part of the process of duplicating the bilobe and FPC. This involves a dramatic rotation of the newly matured basal body that allows the new flagellum to extend without impinging on the old (Lacomble *et al.*, 2010). The new FAZ is also initiated at this point and extends 1–2 μm behind the growing flagellum, adhering it to the cell body (Kohl *et al.*, 1999). The new FAZ continues to extend as the kinetoplast and nucleus duplicate. The cytokinetic furrow initiates from the tip of the new FAZ, creating a precisely positioned furrow that partitions the duplicated organelles to produce two daughter cells (Ploubidou *et al.*, 1999; Hammarton *et al.*, 2003; Tu and Wang, 2004). This directly links the correct assembly and positioning of the new flagellum to the completion of cytokinesis. Perturbing flagellar positioning by depleting FAZ or bilobe components causes cytokinetic defects (He *et al.*, 2005; Bonhivers *et al.*, 2008; Vaughan *et al.*, 2008; Ikeda and de Graffenried, 2012).

Despite a precise morphological understanding of how flagellar inheritance proceeds in trypanosomes, very little is known about the signaling pathways that coordinate these events during cell division. A NimA-related protein kinase homologue is essential for proper basal body duplication, whereas components of the chromosomal passenger complex (CPC) and the *T. brucei* Aurora kinase appear to leave the nucleus late in division to select a site for furrow ingression (Pradel *et al.*, 2006; Li *et al.*, 2008a, 2009). One candidate for a higher-level orchestrator of this process is *T. brucei* polo-like kinase (TbPLK), the single polo-like kinase homologue found in trypanosomes (Kumar and Wang, 2006; Hammarton *et al.*, 2007a; de Graffenried *et al.*, 2008). During cell division, TbPLK first appears on the maturing basal body and then migrates to the bilobe/FPC as they duplicate (Ikeda and de Graffenried, 2012). The kinase subsequently localizes to the tip of the new FAZ and the FC as these structures position the new flagellum. Depletion or inhibition of TbPLK causes defects in basal body segregation and new FPC/bilobe assembly and blocks the initiation and extension of the new FAZ (de Graffenried *et al.*, 2008; Ikeda and de Graffenried, 2012; Lozano-Núñez *et al.*, 2013).

Considering its importance in many different stages of flagellar inheritance, it is likely that understanding how TbPLK interacts with its substrates and binding partners would be an excellent approach to developing a mechanistic understanding of this process. However, many of the PLK substrates found in other organisms, such as Cdc25 and Bub1, appear to be absent in trypanosomes (Yu *et al.*, 2012). This is consistent with the fact that the kinase plays divergent roles in trypanosomes compared with other organisms, in which polo homologues are responsible for chromosome congression and other mitotic events (Archambault and Glover, 2009; Zitouni *et al.*, 2014). These different roles are likely to be reflected by novel trypanosome-specific substrates and interactors. Although we recently identified the calcium-binding protein TbCentrin2 as a viable TbPLK substrate, few other candidates are evident (de Graffenried *et al.*, 2013).

In this work, we use phosphoproteomics and proximity-dependent biotinylation (BioID) to identify potential TbPLK binding partners and substrates. These approaches yield both new and previously identified components of the basal body, bilobe, FPC, and FAZ, which may play important roles in TbPLK signaling pathways. Among our candidates, we identify a FAZ protein that is essential for maintaining the kinetoplast on the posterior side of the nucleus similar to another recently described FAZ protein. We describe the first known component of the FC and show that this structure is not essential for flagellar positioning, as previously hypothesized. We

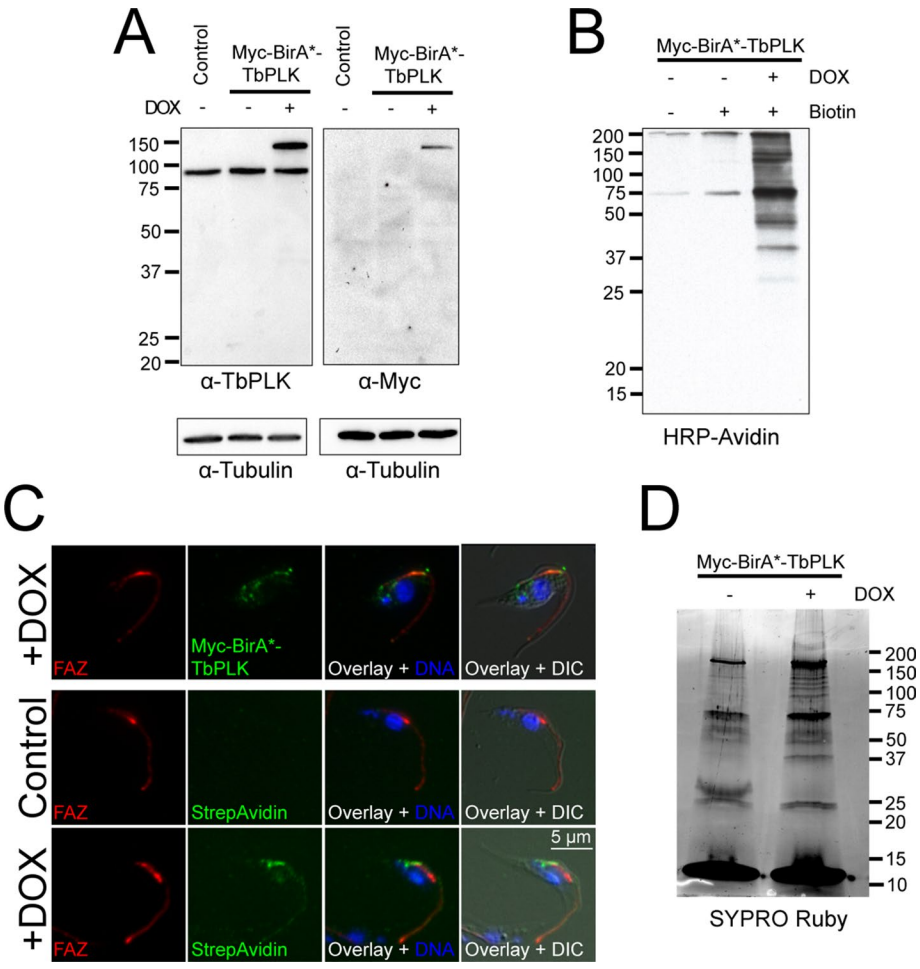

FIGURE 2: Characterization of the Myc-BirA*-TbPLK cell line. (A) Cells carrying doxycycline-inducible Myc-BirA*-TbPLK were treated with 20 ng/ml doxycycline (+) or a vehicle control (–), and then their lysates were probed with antibodies against TbPLK and Myc. Wild-type cells (control) were included as a control. (B) Myc-BirA*-TbPLK cells were treated (+) with 20 ng/ml doxycycline (DOX), biotin, or vehicle control (–), and then their lysates were probed with HRP-streptavidin to detect biotinylation. (C) Myc-BirA*-TbPLK cells were treated (+DOX) with doxycycline or a vehicle control (Control) and labeled with antibodies against the FAZ (FAZ; red) and either anti-Myc (Myc-BirA*-TbPLK; green) or Dylight 488–conjugated streptavidin (StrepAvidin; green), as well as with DAPI to label DNA (DNA; blue). (D) Myc-BirA*-TbPLK cells were incubated with biotin and either doxycycline (+) or a vehicle control (–), followed by lysis and incubation with streptavidin beads. The beads were washed, and 10% of the bound material was eluted and run on an SDS–PAGE gel, which was then imaged using SYPRO ruby.

also identify a protein that localizes to the tip of the new FAZ that is necessary for both initiation of cytokinesis and recruiting TbPLK to the new FAZ. This list of potential TbPLK substrates and interactors will allow us to dissect TbPLK function at different cellular locations and establish mechanisms by which the kinase controls inheritance of the flagellum.

RESULTS

Identification of potential TbPLK binding partners using BioID

Previous work in other organisms identified PLK interactors using immunoprecipitation and by using the C-terminal phosphopeptide-binding domain of the kinase, known as the polo-box, as an affinity reagent (Lowery *et al.*, 2007; Snead *et al.*, 2007; Bastos and Barr, 2010). These methods are less likely to be successful in trypanosomes because many interactors are expected to be components of the cytoskeleton, which are difficult to solubilize under conditions that would preserve binding to TbPLK; moreover, the polo-box domain of TbPLK lacks key conserved residues involved in phosphospecific binding (Yu *et al.*, 2012). To overcome these issues, we chose to use the recently established BioID method to identify proteins that neighbor TbPLK. BioID uses a mutant of the bacterial biotin ligase BirA that generates highly reactive AMP-biotin and releases it into cytoplasm, where it rapidly reacts with free lysine residues on nearby (within 10–12 nm) proteins (Roux *et al.*, 2012). Fusing this BirA mutant, termed BirA*, to a protein of interest leads to the biotinylation of the proteins in close proximity to the fusion. The biotinylated proteins can then be solubilized under denaturing conditions and captured using streptavidin beads.

BioID was recently used in *T. brucei* to identify a host of new bilobe components by fusing BirA* to the bilobe protein MORN1 (Morriswood *et al.*, 2009, 2013). The plasmids and protocols established for MORN1 gave us a good starting point for performing BioID with TbPLK. We generated a myc-BirA*-TbPLK fusion in the doxycycline-inducible vector pLEW100 and integrated it into cells (29-13) that allow doxycycline-inducible expression (Wirtz *et al.*, 1999). We were able to isolate clones that express detectable levels of BirA*-TbPLK upon addition of as little as 10 ng/ml doxycycline. We chose to use 20 ng/ml doxycycline for all our further work because this level of induction produced levels of BirA*-TbPLK that were similar to those with the endogenous kinase, and cell growth was not affected by this level of expression (Figure 2A and Supplemental Figure S1). When lysates from induced and uninduced conditions were probed with horseradish peroxidase (HRP)–streptavidin, a clear increase in biotinylated proteins could be seen upon addition of 50 μM biotin and the induction of the BirA*-TbPLK (Figure 2B). Induced and uninduced cells were fixed and labeled with Dylight 488–streptavidin to detect biotinylated proteins within the cell (Figure 2C). Specific signal along the basal body, bilobe, and FAZ was seen in cytoskeletal preparations from induced cells.

With these preliminary data, we decided to conduct large-scale streptavidin pulldowns on induced and uninduced samples. Approximately 2×10^9 cells were incubated with 20 ng/ml doxycycline or vehicle control for 18 h, followed by lysis in ionic detergent. Pulldowns were then performed with streptavidin beads, followed by a series of stringent washes (Figure 2D). The bound proteins were eluted by on-bead tryptic digest, and the released peptides were identified by liquid chromatography–tandem mass spectrometry (LC-MS/MS). This protocol was repeated three times to assess the reproducibility of the streptavidin pulldown. Proteins that showed at least one unique peptide in each induced sample and had

Gene ID	Screen hit	Location	Notes
Tb927.1.1890	BioID WCL	NUP	
Tb927.10.14320	BioID WCL, P	FAZ	FAZ9; Sunter *et al.* (2015)
Tb927.11.11650	BioID WCL, P	BB	
Tb927.10.840	BioID WCL, P	FAZ	FAZ6; Sunter *et al.* (2015)
Tb927.11.15990	BioID WCL, P	NUP	
Tb927.9.7690	BioID WCL, S	CYTO	
Tb927.11.11080	BioID WCL	NUP	
Tb927.3.3130	BioID WCL	CYTO	
Tb927.11.3300	BioID WCL	FAZ	
Tb927.3.4960	BioID WCL, P	CYTO	
Tb927.10.3010	BioID WCL, P	BILOBE	Morriswood *et al.* (2013)
Tb927.10.15750	BioID WCL, P; SILAC; iTRAQ	BB	p197; Gheiratmand *et al.* (2013)
Tb927.6.890	BioID WCL, P	NUP	
Tb927.11.980	BioID WCL, P	NUP	
Tb927.9.6460	BioID WCL	NUP	
Tb11.01.2730	BioID WCL, P	BILOBE	
Tb927.7.7400	BioID WCL, P	BB	
Tb927.10.12860	BioID WCL	CYTO	
Tb927.7.2640	BioID WCL, P, S	CORSET	
Tb927.11.15800	BioID WCL, P, S; SILAC; iTRAQ	FAZ	TOEFAZ1; this work
Tb927.4.2000	BioID WCL, S	CYTO	
Tb927.11.6440	BioID WCL, S	CYTO	
Tb927.10.5810	BioID WCL, S	CYTO	
Tb927.7.3880	BioID WCL, S	BB	
Tb927.3.4400	BioID WCL, P	BB	
Tb927.7.6620	BioID WCL	CYTO	
Tb927.1.3200	BioID WCL	CYTO	
Tb927.5.2500	BioID WCL	BILOBE	
Tb927.9.8200	BioID WCL	NUC	
Tb927.7.2680	BioID WCL	CYTO	
Tb927.10.14890	BioID WCL	CYTO	
Tb927.10.8820	BioID WCL, P; SILAC; iTRAQ	BILOBE	Morriswood *et al.* (2013)
Tb927.7.3330	BioID WCL, P	FAZ	Morriswood *et al.* (2013)
Tb927.10.1450	BioID WCL, P	BILOBE	Morriswood *et al.* (2013)
Tb927.10.850	BioID WCL, P	BILOBE	Morriswood *et al.* (2013)
Tb927.10.14520	BioID P	BB	
Tb927.4.2070	BioID P	CYTO	
Tb927.9.5750	BioID P	CYTO	
Tb927.11.10660	BioID P	BB	
Tb927.4.4180	BioID P	BILOBE	
Tb927.11.5640	BioID P; SILAC; iTRAQ	COLLAR	
Tb927.11.8950	BioID P	BILOBE	LRRP1; Zhou *et al.* (2010)
Tb927.2.4230	BioID P	NUP	NUP-1; Dubois *et al.* (2012)
Tb927.10.10360	BioID P	CORSET	MARP1; Schneider *et al.* (1988)
Tb927.4.2080	BioID P	FAZ	CC2D; Zhou *et al.* (2011)
Tb927.9.13820	BioID P	BB	KMP-11; Li and Wang (2008)
Tb927.11.16050	BioID S	CYTO	
Tb927.9.10490	BioID S	CYTO	
Tb927.10.10890	BioID S	CYTO	
Tb927.4.2740	BioID S	CYTO	
Tb927.6.1520	BioID S	SURFACE	
Tb927.11.2610	BioID S	CORSET	
Tb927.5.1650	BioID S	CYTO	
Tb927.10.1450	BioID S	BILOBE	
Tb927.8.7070	SILAC; iTRAQ	FAZ	
Tb927.3.4250	SILAC; iTRAQ	CYTO	
Tb927.5.3460	SILAC; iTRAQ	FAZ	
Tb927.11.1340	SILAC	CNTR	FC1; this work
Tb927.10.5460	SILAC	CYTO	
Tb927.9.7520	SILAC	CYTO	
Tb927.10.2240	SILAC; iTRAQ	CYTO	
Tb927.10.7210	SILAC; iTRAQ	FAZ	
Tb927.1.4400	SILAC; iTRAQ	BILOBE	

The BioID hits are separated into proteins found in the whole-cell lysate (WCL), pellet (P), or supernatant (S) fractions. The phosphoproteomic hits are separated into SILAC or iTRAQ hits. The localization of each protein was established by tagging of the endogenous locus. BB, basal body; COLLAR, flagellar pocket collar; CNTR, flagella connector; CORSET, subpellicular microtubule corset; CYTO, cytoplasmic; NUC, nuclear; NUP, nuclear pore; SURFACE, cell surface.

TABLE 1: Proteins identified in the BioID and phosphoproteomic screens.

minimal or no peptides in the uninduced samples were considered to be specific hits and investigated further. This criterion produced 35 candidate proteins (Table 1 and Supplemental Figure S2). Of interest, five of these proteins were present in the BirA*-MORN1 screen, which was targeted specifically toward identifying new bilobe proteins (Morriswood *et al.*, 2013). This gave us confidence

that our candidates included cytoskeletal proteins that are present on structures to which TbPLK localizes.

We also conducted additional experiments in which the initial cell lysis was performed with mild detergent, which extracts most of the cytoplasmic proteins but keeps the cytoskeleton intact (Morriswood *et al.*, 2013). The resultant lysate was separated by centrifugation into a soluble fraction that contained mostly cytosolic proteins and a pellet fraction containing mostly cytoskeletal proteins. Both fractions were incubated with streptavidin beads, and the bound proteins were identified. This fractionation step gave us information about the solubility of the bound proteins and improved LC-MS/MS detection by separating the biotinylated proteins into two samples, allowing us to identify new proteins that were not identified when the whole-cell lysate was analyzed. This approach yielded many of the same proteins seen in the whole-cell approach, but we found 11 new potential binding partners in the pellet fraction and 8 in the soluble fraction (Table 1 and Supplemental Figure S2). The bilobe protein LRRP1, the FAZ protein CC2D, and the basal body protein KMP11 were also identified, showing that we were identifying components of structures to which TbPLK localizes during the cell cycle (Zhou *et al.*, 2010, 2011; Gheiratmand *et al.*, 2013).

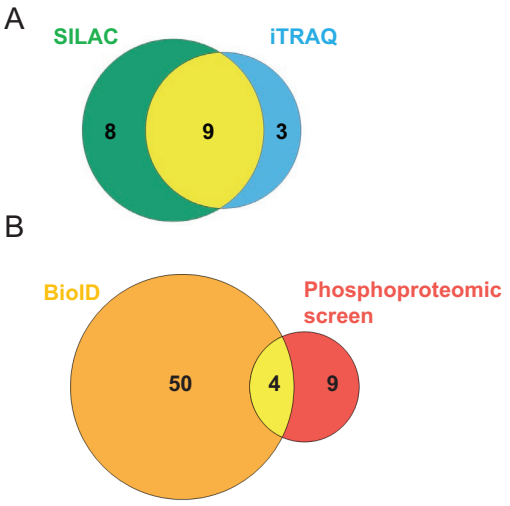

FIGURE 3: Analysis of the BioID and phosphoproteomic screens. (A) Venn diagram showing overlap of the regulated phosphopeptides identified in the iTRAQ and SILAC screens. (B) Venn diagram showing overlap of the proteins identified in the BioID and phosphoproteomic screens.

Identification of potential TbPLK substrates using phosphoproteomics

The divergent localization and function of TbPLK are likely reflected by novel substrates. Polo-like kinases do not have strong substrate recognition motifs (E/D/N-X-S/T), and the priming phosphorylation that targets the kinase to its substrates does not fall within a strongly conserved sequence (Lowery *et al.*, 2007; Snead *et al.*, 2007; Yun *et al.*, 2009; Dou *et al.*, 2011). To overcome these problems, we used two different quantitative phosphoproteomic methods to identify potential TbPLK substrates. Both methods take advantage of an analogue-sensitive TbPLK cell line that we generated recently (Lozano-Núñez *et al.*, 2013). This method sensitizes kinases via a mutation in the ATP-binding site so that they can bind a modified general kinase inhibitor (Bishop *et al.*, 2000; Burkard *et al.*, 2007). The modification makes the inhibitor capable of inhibiting only kinases with the mutation in their ATP-binding site. In wild-type cells, the modified inhibitor, known as 3MB-PP1, has no effect on growth, showing that the drug cannot inhibit any essential endogenous kinases. In cells in which the accommodating mutation has been installed within TbPLK, 3MB-PP1 treatment blocks cell division within 6 h of treatment. These results show that the TbPLKas cell line responds to drug treatment and that the drug has no effect on wild-type cells, suggesting that any off-target effects of 3MB-PP1 are minimal (Lozano-Núñez *et al.*, 2013).

We sought to identify in vivo TbPLK substrates by inhibiting TbPLK in cells and monitoring changes in phosphorylation using quantitative MS methods. We used two distinct approaches that complement one another. First, we used a stable isotope labeling by amino acids in cell culture (SILAC) approach in asynchronous cultures, which requires labeling one sample with $^{13}C/^{15}N$-labeled arginine and lysine and the other with unlabeled amino acids (Kean *et al.*, 2012; Urbaniak *et al.*, 2012). One culture is treated with 5 μM 3MB-PP1 to inhibit TbPLK and block phosphorylation, and the second sample is treated with a vehicle control. To improve our detection of changes in TbPLK phosphorylation at specific time points, we used a second proteomic approach (isobaric tags for relative and absolute quantitation [iTRAQ]), which does not rely on metabolic labeling, coupled with a double-cut elutriation procedure to synchronize cells at the beginning of the cell cycle (Archer *et al.*, 2011). After 1.5 h in culture, the cells were treated with 3MB-PP1 or a vehicle control. During this time, the kinase is predominantly on the bilobe; we previously showed that inhibiting the kinase at this point blocks bilobe duplication. Bilobe-resident substrates should show diminished levels of phosphorylation if TbPLK is inhibited at this time (Lozano-Núñez *et al.*, 2013).

We performed five SILAC and two iTRAQ experiments to identify novel TbPLK substrates. The SILAC experiments yielded 13 proteins for which specific phosphosites were more than twofold down-regulated, whereas the iTRAQ experiments identified nine proteins with down-regulated phosphosites (Table 1 and Supplemental Figure S3). Overall, 20 regulated phosphosites were identified, nine of which were identified in both phosphoproteomic approaches (Figure 3A). Of the 13 possible substrates identified, four of the proteins are also present in the BioID screen, providing additional evidence that they are TbPLK substrates (Figure 3B). Two of these proteins had been previously identified in other screens: Tb927.10.15750, termed p197, is a component of the tripartite attachment complex that anchors the basal body to the kinetoplast, and Tb927.10.8820 is a bilobe component identified in the MORN1 BioID screen (Gheiratmand *et al.*, 2013; Morriswood *et al.*, 2013).

Characterization of potential TbPLK binding partners and substrates

Identification of bilobe, basal body, and FAZ components among our candidates gave us confidence that many of the unidentified proteins would localize to the these compartments. However, most of the candidate proteins lacked conserved domains or homology to known proteins, and so it was difficult to choose a subset for further study. Therefore we chose to endogenously tag each protein at its N-terminus with a triple-Ty1 epitope tag so that its localization could be established (Bastin *et al.*, 1996; Morriswood *et al.*, 2009). Endogenous tagging was essential to maintain cell cycle regulation of the candidate proteins and express the proteins at levels comparable to their wild-type levels. Locus PCR and Ty1 Western blotting were used to confirm correct targeting of the triple-Ty1 tag. Once the cell lines were generated and confirmed, the localization of the Ty1 fusions was established by immunofluorescence, and the

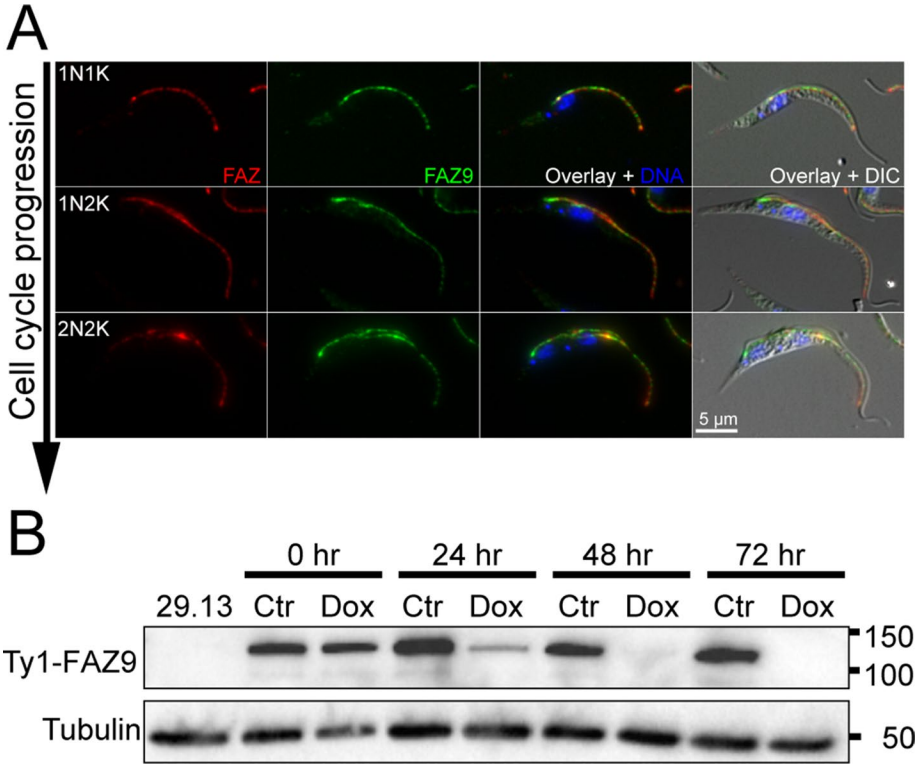

FIGURE 4.: FAZ9 is a component of the FAZ. (A) Cells expressing 3X-Ty1-FAZ9 from the endogenous locus were fixed with methanol and labeled with an antibody against the FAZ (FAZ; red), anti-Ty1 (FAZ9; green), and DAPI to label the DNA (DNA; blue). The three rows show cells as they progress through the cell cycle. (B) FAZ9 RNAi cells expressing 3X-Ty1-FAZ9 from the endogenous locus were treated with doxycycline (DOX) or a vehicle control (Ctr). Cells were collected every 24 h to monitor FAZ9 depletion by Ty1 Western blotting, using tubulin as a loading control.

pattern was compared with antibodies to markers of different cytoskeletal compartments (Supplemental Figure S4). We were able to select stable cell lines expressing detectable Ty1 fusions for all of our candidate proteins except for Tb927.3.4400, which required the relocation of the Ty1 tag to the C-terminus before viable cell lines could be established.

Our localization screen showed that many of our candidate proteins were part of cytoskeletal compartments to which TbPLK is recruited during cell division (Figure 3C and Supplemental Figure S4). These include components of the bilobe (11), FAZ (nine), and basal body (eight). More unique identifications included a new flagellar pocket collar protein (Tb927.11.5640), which has only a single known protein component, BILBO1, and the first identified component of what appears to be the flagella connector (Tb927.11.1340; further evidence for this is provided later in this article). We also identified a small number of proteins (four) that look like they are associated with the plasma membrane or the subpellicular microtubules. Twenty-two of the proteins showed primarily cytoplasmic labeling. When previously identified proteins are considered, our screen identified 40 cytoskeletal proteins localizing to a diverse set of compartments. The four candidates that were present in both our phosphoproteomic and BioID screens localized to the basal body (p197), FAZ (Tb927.11.15800), bilobe (Tb927.10.8820), and FPC (Tb927.11.5640).

As a follow-up to our localization screen, we chose a subset of the candidate proteins and performed more in-depth localization experiments and RNA interference (RNAi) using an inducible long hairpin RNAi (lhRNAi) strategy (Kalidas *et al.*, 2011). We integrated our Ty1 endogenous tagging cassettes for each protein into their cognate RNAi cell line so that we could directly monitor depletion of the proteins by Western blotting (Chanez *et al.*, 2006). We chose to focus on three candidates: Tb927.10.14320, Tb927.11.1340, and Tb927.11.15800. Our screen localization results suggested that the three proteins were cytoskeletal components, and none of them had been characterized previously.

A FAZ component plays an important role in the positioning of the kinetoplast

Tb927.10.14320 is a 121-kDa protein that was identified in our BioID screen. The protein contains an unstructured N-terminal domain and a C-terminal domain consisting of a series of armadillo repeats similar to those found in β-catenin (Peifer *et al.*, 1994; Huber *et al.*, 1997). These repeats can form extended binding surfaces and are found in proteins that form linkages with cytoskeletal elements. This protein was recently identified as a FAZ component in a proteomic screen and was named FAZ9 (Sunter *et al.*, 2015). Anti-Ty1 labeling showed that tagged FAZ9 localized to the FAZ throughout the cell cycle (Figure 4A), confirming the localization of this protein. At the start of cell division, trypanosomes contain a single copy of the nucleus and kinetoplast (1N1K). Kinetoplast duplication occurs first (1N2K), followed by karyokinesis (2N2K). FAZ9 appears to be slightly more concentrated on the posterior end of the FAZ than along the rest of the structure.

FAZ9 depletion was complete within 72 h of induction of RNAi (Figure 4B). Cell counting showed no change in growth within 4 d of RNAi induction, although the depleted cells showed a small decrease in growth at later time points (Supplemental Figure S5). Differential interference contrast (DIC) and 4′,6-diamidino-2-phenylindole (DAPI) imaging at days 1–4 after RNAi induction showed no substantial changes in cell cycle distribution or DNA content (Supplemental Figure S6). However, it was apparent that in FAZ9-depleted cells, the kinetoplast was now located on the anterior side of the nucleus (Figure 5, A and B). This relocation normally occurs in PCFs during their migration from the fly midgut to the salivary glands while the parasite undergoes several morphological changes, including an asymmetric cell division that produces a small parasite with an anteriorly placed kinetoplast (Sharma *et al.*, 2008; Rotureau *et al.*, 2012). A recent report showed that depletion of another FAZ protein known as ClpGM6 causes trypomastigotes to become epimastigotes, along with an overall shortening of the cell body and the new FAZ (Hayes *et al.*, 2014).

To test whether FAZ9 had any effect on the length of the new FAZ, we depleted the protein for 4 d and labeled cells with anti-FAZ1, which labels the filament, and 1B41, which labels the microtubule quartet (Gallo *et al.*, 1988; Kohl *et al.*, 1999; Vaughan *et al.*, 2008). In FAZ9-depleted cells, the 1B41 signal became more disperse, labeling only the beginning and the end of the FAZ, along with the tip of the new FAZ in cells undergoing division (Figure 5C). Because of this

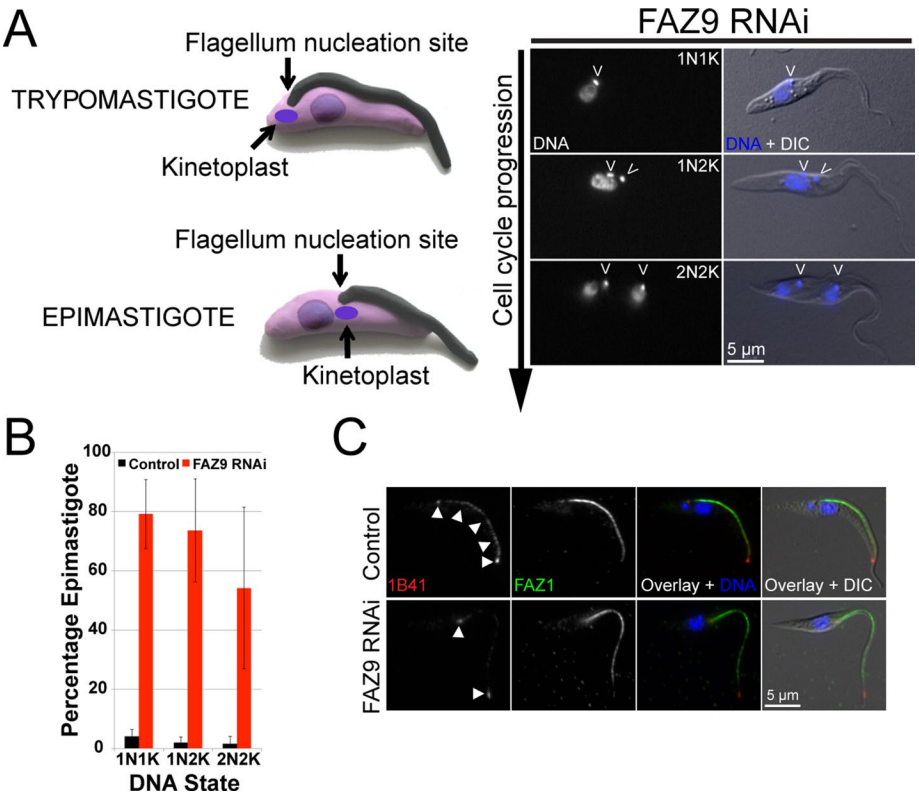

FIGURE 5: FAZ9 depletion causes relocation of the kinetoplast. (A) Cells that had been depleted of FAZ9 for 4 d were labeled with DAPI to label DNA and evaluated by fluorescence and DIC imaging. In the first column, the DNA channel is shown in monochrome, with the kinetoplasts marked by open arrowheads. In the second column, the DNA channel (DNA; blue) is merged with DIC in monochrome. The rows show cells as the progress in the cell cycle. (B) Quantitation of kinetoplast positioning in cells labeled as in A. (C) Control and FAZ9-depleted cells were fixed and labeled with 1B41 (1B41; red), anti-FAZ1 (FAZ1; green), and DAPI to label the DNA. Cells were evaluated by fluorescence and DIC imaging. Arrowheads show the 1B41 labeling, which is suppressed in FAZ9-depleted cells.

phenotype, we chose to use the FAZ1 signal for further quantitation. Measurement of FAZ length in FAZ9-depleted cells at the 1N1K cell cycle stage showed that the structure maintained the same length as uninduced cells (control, 14.3 ± 1.6 µm; FAZ9 RNAi, 15.1 ± 1.7 µm). This differs substantially from ClpGM6 depletion, where newly assembled FAZs are shorter but concentrate the same amount of filament components into the smaller structure, producing brighter FAZ labeling.

A component of the FC is essential for connection of the new and old flagella during cell division

We next focused on Tb927.11.1340, which contains an N-terminal kinase domain and a C-terminal domain of unknown function. This protein was identified as a putative TbPLK substrate in our SILAC phosphoproteomic screen, with two potential phosphosites (T888 and S890) in the C-terminal domain that have been previously identified (Urbaniak *et al.*, 2013). Ty1 tagging showed that the protein localizes to the connection point between the new and old flagella, which is the location of the flagella connector in PCFs. This cytoskeletal structure has no known components, although TbPLK does transiently localize to the FC during cell division (Ikeda and de Graffenried, 2012). To confirm the localization pattern, we stained the Ty1-tagged cells with AB1, a monoclonal antibody against an unknown protein that labels the FC (Figure 6A; Briggs *et al.*, 2004). The Ty1-tagged protein labeled the FC throughout cell division, although the Ty1 signal was very slightly offset from the AB1 signal, suggesting that the protein may localize to a different domain of the FC. We decided to call this protein FC1 to reflect its localization. At early cell cycle stages, FC1 appears in the posterior of the cell in what is likely the flagellar pocket, where the connection between the two flagella is established. Once the new flagellum has emerged onto the cell surface, the FC1 puncta localizes to the contact point of the two flagella and remains there as the new flagellum extends along the old one. The FC1 signal disappears once the two flagella disconnect just before cytokinesis. Colabeling with antibodies against TbPLK shows that the FC1 signal colocalizes with a portion of the TbPLK signal early in the cell cycle that is present at the tip of the new flagellum (Figure 6B). We previously showed that this TbPLK labeling is present on the FC by immuno-electron microscopy on negatively stained extracted cytoskeletons (Ikeda and de Graffenried, 2012). The TbPLK signal on the FC decreases later in the cell cycle, once the basal bodies begin to separate.

RNAi against FC1 showed efficient depletion of the protein after 48 h by Western blotting of the Ty1-FC1 fusion, but no cell growth defect was observed even after 7 d of RNAi (Figure 7A and Supplemental Figure S7). The DNA state and general morphology of FC1-depleted cells were not disrupted (Supplemental Figure S8), although we did observe disconnection of the tip of the new flagellum from the old flagellum (Figure 7B). This disconnection was evident at the 1N2K (48%) and 2N2K (59%) stages of cell division (Figure 7C). Of importance, the new flagellum remained adhered to the cell body. FC1 RNAi cells were induced with doxycycline or vehicle control and then fixed and processed for scanning electron microscopy so that the state of flagella connection could be established at higher resolution at early and late stages of cell division. In vehicle control cells, the new flagellum was clearly in direct contact with the old flagellum both when the new flagellum had just emerged from the flagellar pocket and when it had extended along the cell surface, which would allow the transmission of positional information (Figure 7D). In FC1-depleted cells, it is difficult to tell whether the newly emerged flagellum is connected to the old flagellum, although the tip of the new flagellum appears to be free. In later stages of cell division, there was a clear gap of ~500 nm separating the two flagella, although the new flagellum appeared to be correctly positioned along the cell body with the same helical pattern seen in uninduced cells. This result argues that the biogenesis of the FC requires FC1 and that the FC may be dispensable for the correct positioning of the new flagellum during cell division.

A protein localizing to the tip of the extending FAZ is essential for cytokinesis

We next looked at the protein Tb927.11.15800, which contains two distinct domains—an N-terminal region that has similarities to

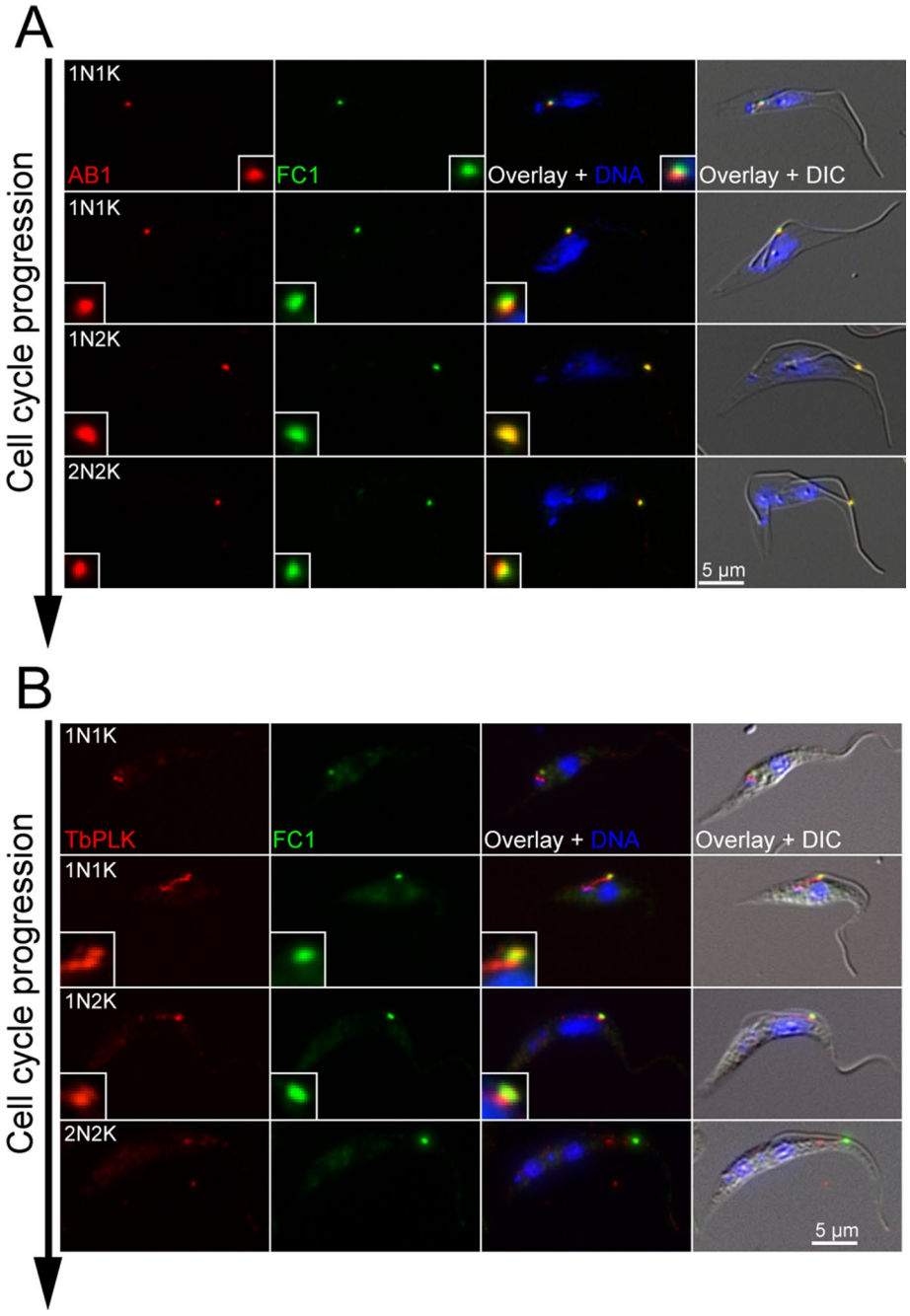

FIGURE 6: FC1 is a component of the flagella connector. (A) Cells expressing 3X-Ty1-FC1 from the endogenous promoter were fixed and labeled with anti-Ty1 (FC1; green), an antibody against the FC (AB1; red), and DAPI (DNA; blue). The cells were visualized using fluorescence and DIC microscopy. The rows show different cells at progressively later points of the cell cycle. (B) The same cells as in A were fixed and labeled with anti-Ty1 (FC1; green), antibodies against TbPLK (TbPLK; red), and DAPI (DNA; blue). The rows show different cells at progressively later points of the cell cycle. Insets show threefold magnifications of the area surrounding the FC1 signal.

tricohyalins, which provide mechanical stability in epithelia, and a C-terminal domain that contains a zinc finger (Steinert *et al.*, 1998, 2003). This protein was identified in both our BioID and phosphoproteomic screens and has four potentially regulated phosphosites (S15, S17, S18, and S33) in its N-terminal domain. The first three phosphosites were previously identified in another phosphoproteomic screen (Urbaniak *et al.*, 2013). The protein first appears in cells in which TbPLK is concentrated on the anterior end of the bilobe structure, which is when the tip of the new FAZ becomes visible (Figure 8A). TbPLK and the protein colocalize at the tip of the new FAZ as the structure continues to extend, until the TbPLK signal begins to decline just before cytokinesis (Figure 8B). We chose to name the protein TOEFAZ1 (Tip Of Extending FAZ) to reflect its localization pattern. Cleavage furrow ingression appears to occur from a point on the anterior side of the remaining TOEFAZ1 puncta late in the cell cycle.

Depletion of TOEFAZ1 is essentially complete after 24 h of RNAi induction (Figure 9A). Cell division was compromised within 2 d of initiation of RNAi, with the cells fully arresting growth by day 5 (Figure 9A). DIC and DAPI imaging after 1 d of RNAi showed a pronounced decrease in 1N1K cells and concomitant increase in 2N2K cells, with no change in 1N2K cells (Figure 9B). In half of the TOEFAZ1-depleted 2N2K cells, the tip of the new flagellum had detached from the old flagellum, which we rarely observed in uninduced samples (Figure 9, C and D). These changes were more pronounced 2 d after TOEFAZ1 depletion, with 1N1K cells now comprising <10% of the population. The number of 1N2K cells decreased, whereas the number of 2N2K cells remained high. Multinucleated cells were the most common, comprising 37% of the population (Figure 9C). Cells lacking nuclei and cells containing additional kinetoplasts were also evident at this time point. Attempts to quantitate DNA content at later time points were not feasible due to the incredibly high number of multinucleated cells with complex morphologies.

Considering the localization of TOEFAZ1 during cell division and its apparent importance in cytokinesis, we stained TOEFAZ1-depleted and control cells with antibodies against the FAZ and TbPLK. In uninduced cells, TbPLK localization followed its normal progression, starting on the basal body and bilobe in the posterior of 1N1K cells early in division, then progressing toward the anterior end of the cell via the tip of the new FAZ and the FC during the late 1N1K and 1N2K states, until disappearing in 2N2K cells just before cytokinesis (Figure 10, A and B; Ikeda and de Graffenried, 2012). In TOEFAZ1-depleted cells, TbPLK appeared at the basal body and bilobe in 1N1K cells that were just beginning to divide. However, TbPLK did not appear to localize to the tip of the new FAZ in late 1N1K cells, and the kinase was absent from the new FAZ tip in 1N2K and 2N2K cells as well (Figure 10, A and B). In contrast, TbPLK recruitment to the FC appeared to proceed normally. In a subset of 2N2K cells—frequently those with detached new flagellum tips—TbPLK was associated with the duplicated basal bodies

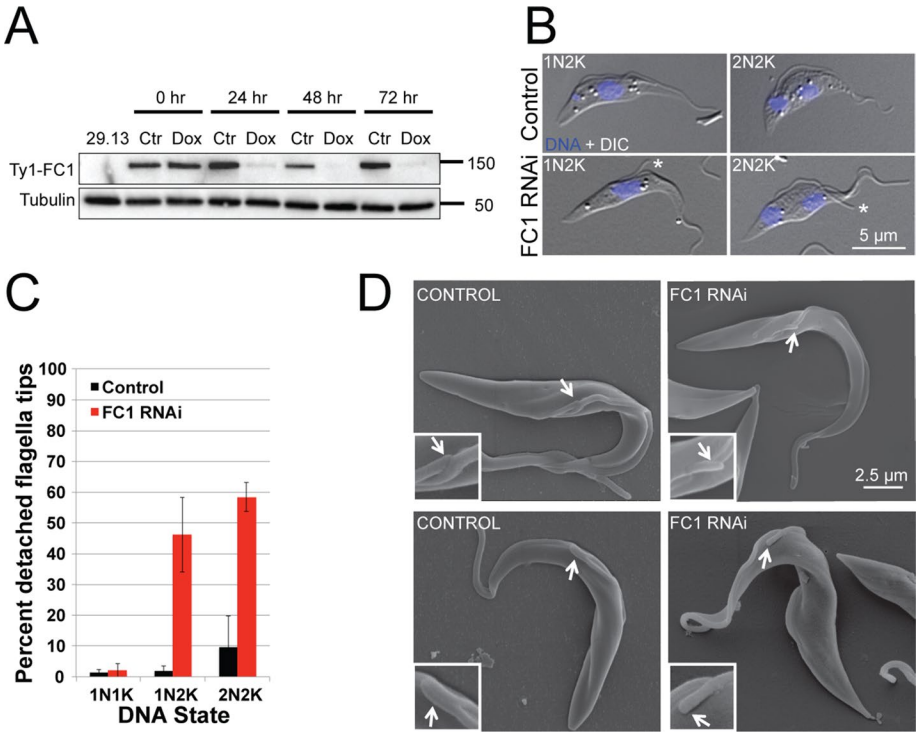

FIGURE 7: FC1 depletion causes a loss of connection between the new and old flagella. (A) FC1 RNAi cells expressing 3X-Ty1-FC1 from the endogenous locus were treated with doxycycline (DOX) or a vehicle control (Ctr). Cells were collected every 24 h to monitor FC1 depletion by Ty1 Western blotting, using tubulin as a loading control. (B) Uninduced and cells depleted of FC1 for 2 d were treated with DAPI to label DNA (DNA; blue) and evaluated by fluorescence and DIC imaging. Images of 1N2K and 2N2K cells. Asterisks show detached new flagellar tips. (C) Quantitation of flagellar tip detachment of the data presented in B. (D) Selected scanning electron micrographs of control and FC1-depleted cells at both early and late stages of cell division. The arrows show the tips of the new flagella.

and bilobes, which never occurred in cells containing TOEFAZ1. This phenotype is similar to what occurs upon inhibition of TbPLK, which causes the kinase to localize to the posterior of the cell in 2N2K cells (Lozano-Núñez *et al.*, 2013).

DISCUSSION

Of the 63 proteins identified in our proteomic screens, more than half localized to cytoskeletal compartments to which TbPLK localizes during cell division, such as the basal body, bilobe, and FAZ. Although these cytoskeletal components are strong candidates for involvement in TbPLK signaling pathways due to their localization, further work is necessary to confirm that they are direct substrates and/or binding partners of the kinase. Note that 11 of the 19 regulated phosphosites fell within the PLK consensus sequence identified for the yeast and mammalian kinases, which indicates that they are more likely to be direct substrates if TbPLK has maintained the same specificity (Johnson *et al.*, 2007; Snead *et al.*, 2007; Murugan *et al.*, 2011). All of the hits from our synchronized cell iTRAQ screen appeared among our SILAC hits, which provides additional evidence that these proteins are components of TbPLK signaling pathways. It is unknown whether TbPLK binds to phosphorylated proteins using the polo-box domain, as is the case with other PLK homologues, although most of our candidates contain the minimal serine-proline motifs that could function as substrates for upstream kinases to generate potential binding sites (Elia *et al.*, 2003; Yun *et al.*, 2009). Considering the lack of known TbPLK binding partners, the screen hits could be further studied biochemically to identify direct interactors, which could then be used to dissect the mechanism of kinase recruitment. If TbPLK has evolved a novel mechanism for localization, it would explain how its function has diverged so significantly from that of other PLK homologues (Park *et al.*, 2003; Bashor *et al.*, 2008).

One unexpected result was the identification of several nuclear pore components as potential TbPLK interactors. Although there is no evidence that full-length TbPLK enters the nucleus, it is possible that the kinase comes into the proximity of the nuclear pores as it is migrating throughout the cell, which might explain their presence as BioID hits. An alternative possibility is that these nuclear pore components are also part of the recently identified ciliary pore complex, which functions as a selection filter for entrance into the cilia in mammalian cells (Kee *et al.*, 2012; Obado and Rout, 2012). An analogous flagellar pore complex has not yet been identified in trypanosomes, but if the structure is present, TbPLK may encounter the nuclear pore proteins as it migrates to the FC during production of the new flagellum.

FAZ9, which was identified in our BioID screen, appears to be involved in maintaining cells in the trypomastigote form. In procyclic cells, the kinetoplast is initially found in the posterior of cells that occupy the fly midgut. A highly asymmetric cell division that occurs during the migration of the parasite to the proventriculus and esophagus produces a smaller cell in which the kinetoplast is present on the anterior side of the nucleus (Sharma *et al.*, 2008; Rotureau *et al.*, 2012). This epimastigote form transitions to a slightly longer cell that is associated with the salivary gland epithelium and is able to divide. Depletion of the FAZ protein ClpGM6 produces smaller, epimastigote-like cells (Hayes *et al.*, 2014). Earlier work also showed that knockdown of the protein phosphatase PP1-3 causes kinetoplast rearrangement without affecting the length of the cell body; in this case, the nucleus is found closer to the posterior end of the cell, which leaves the kinetoplast closer to the anterior of the cell (Gallet *et al.*, 2013). FAZ9 depletion causes a rearrangement more similar to PP1-3 because FAZ length remains the same as in control cells.

Our results show that kinetoplast positioning may rely on several different FAZ components. One possibility for how this control is mediated is via the MtQ, which is the only FAZ component that interacts directly with the basal body (Lacomble *et al.*, 2009). It is possible that changes in the FAZ filament affect the length or positioning of the MtQ, which could in turn change the positioning of the basal body and kinetoplast. FAZ9 depletion causes a decrease in FAZ labeling by the antibody 1B41, which is proposed to label an unknown modification of β-tubulin present exclusively on the MtQ. The consequence of this diminished labeling is unknown, although it is likely that the MtQ remains intact. It is also possible that the FAZ plays a role in positioning the nucleus during cell division. The MtQ is associated with an extension of endoplasmic reticulum that is contiguous with the nuclear membrane (Taylor and Godfrey, 1969). This connection may facilitate nuclear separation during cell division and ensure that the nucleus is maintained in the

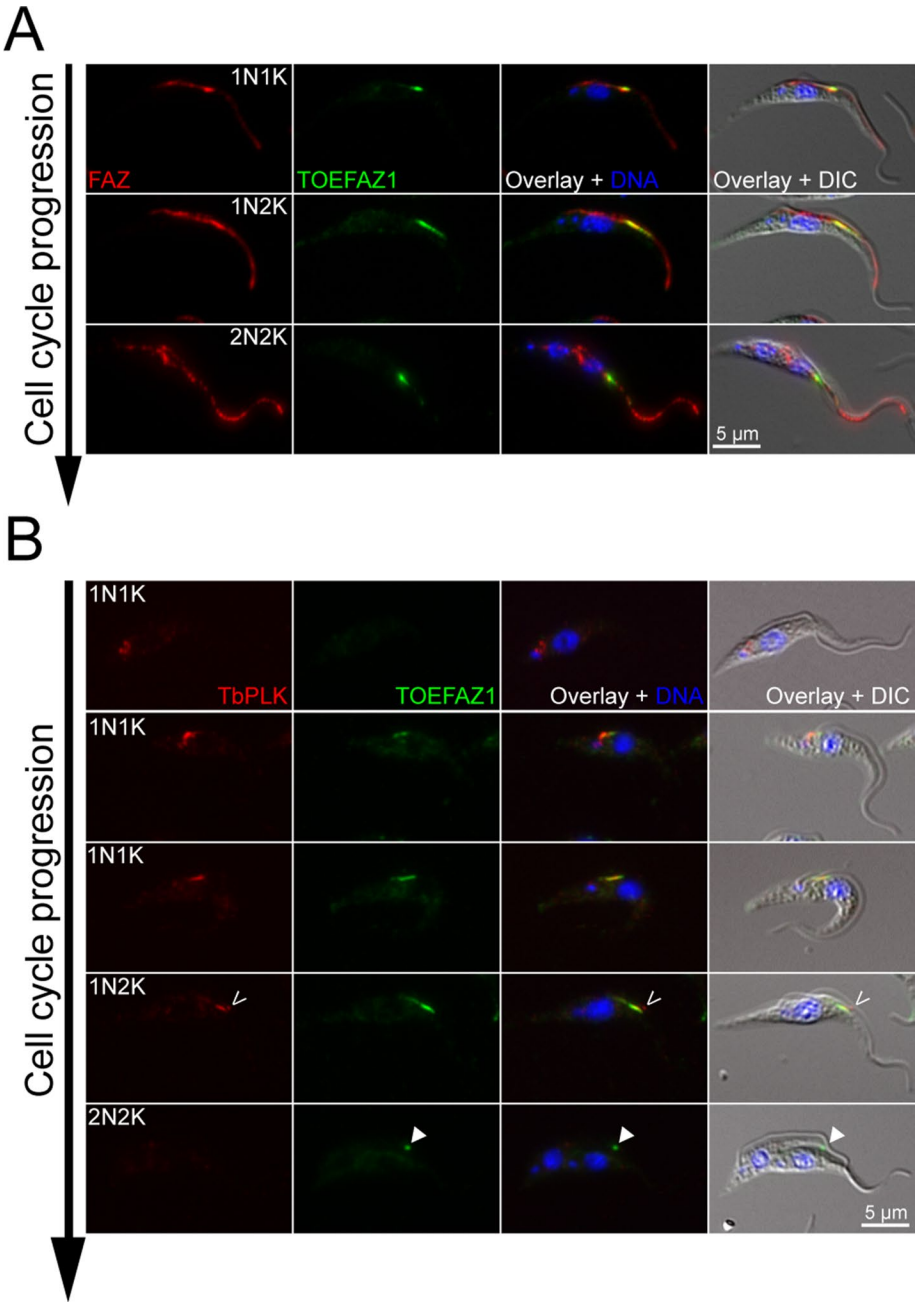

FIGURE 8: TOEFAZ1 localizes to the tip of the new FAZ. (A) Cells expressing 3X-Ty1-TOEFAZ1 from the endogenous promoter were fixed and labeled with an antibody against the FAZ (FAZ; red), anti-Ty1 (TOEFAZ1; green), and DAPI to label the DNA (DNA; blue). The cells were then imaged by fluorescence and DIC microscopy. The rows show different cells at progressively later points of the cell cycle. (B) The same cell line as in A was fixed and labeled with antibodies against TbPLK (TbPLK; red), anti-Ty1 (TOEFAZ1; green), and DAPI to label the DNA (DNA; blue). The rows show different cells at progressively later points of the cell cycle. Empty arrowheads show the TbPLK labeling on the flagella connector, and filled arrowheads show the TOEFAZ1 present late in the cell cycle at the point of cleavage furrow ingression.

correct location. Disruption of this connection could lead to repositioning of the nucleus to a more posterior location, which would produce epimastigotes. We are investigating which of these models best describes the consequence of FAZ9 depletion.

We have identified FC1 as the first component, to our knowledge, of the flagella connector in our TbPLK phosphoproteomic screen. This structure was initially identified morphologically by electron microscopy and proposed to have a cytotactic function that conveyed positional information from the old flagellum to the new one (Moreira-Leite *et al.*, 2001; Briggs *et al.*, 2004). However, no protein components of this structure had been previously identified, so its function could not be tested via methods such as RNAi. Depletion of FC1 causes a loss of the connection between the two flagella tips but does not influence the positioning of the new flagellum or the viability of procyclic trypanosomes. This strongly suggests that the FAZ may play a more prominent role in flagellar positioning than previously believed. The FC is present only in PCFs, whereas in BSFs, the tip of the new flagellum is housed in a groove in the cell surface that is adjacent to the MtQ and the FAZ filament (Hughes *et al.*, 2013). This implies that the correct positioning of the new FAZ may be a more general mechanism for flagellum placement across different life stages. Because positioning the new flagellum is essential for the completion of cell division, it is likely that some redundancy is built into this process. FC1 and TbPLK are both kinases that may be components of a more extensive signaling network. One process that may be under their control is the movement of the FC, which stops once the structure has progressed to approximately half the length of the old flagellum (Davidge *et al.*, 2006). Accommodation of the further extension of the new flagellum appears to occur by separation of the basal bodies and elongation of the cell posterior. The timing and positioning of this event may require FC1 and TbPLK activity.

Our BioID and substrate screens identified TOEFAZ1, which localizes to the tip of the new FAZ as it extends during cell division in a manner similar to TbPLK. Depletion of TOEFAZ1 led to a block in cytokinesis, which argues that the tip of the new FAZ contains a complex that is essential for triggering furrow ingression. This inhibition of cytokinesis is very specific, because at early time points, we observe 2N2K cells that have detached new flagellar tips. This detachment is confined to 2N2K cells, arguing that FC assembly is not defective in TOEFAZ1-depleted cells. Disconnection of the new flagellum from the old one requires dissolution of the FC, which happens after furrow ingression has occurred. It is likely that the 2N2K cells are unable to initiate cytokinesis, but then proceed to flagellar disconnection, which appears to be independent of furrow ingression. The new FAZ tip structure may also contain an Aurora kinase homologue and the chromosomal passenger complex proteins CPC1 and CPC2, which form a complex (Li *et al.*, 2008a,b). These proteins are associated with formation of the mitotic spindle but then exit the nucleus and migrate to a location that is consistent with the tip of the new

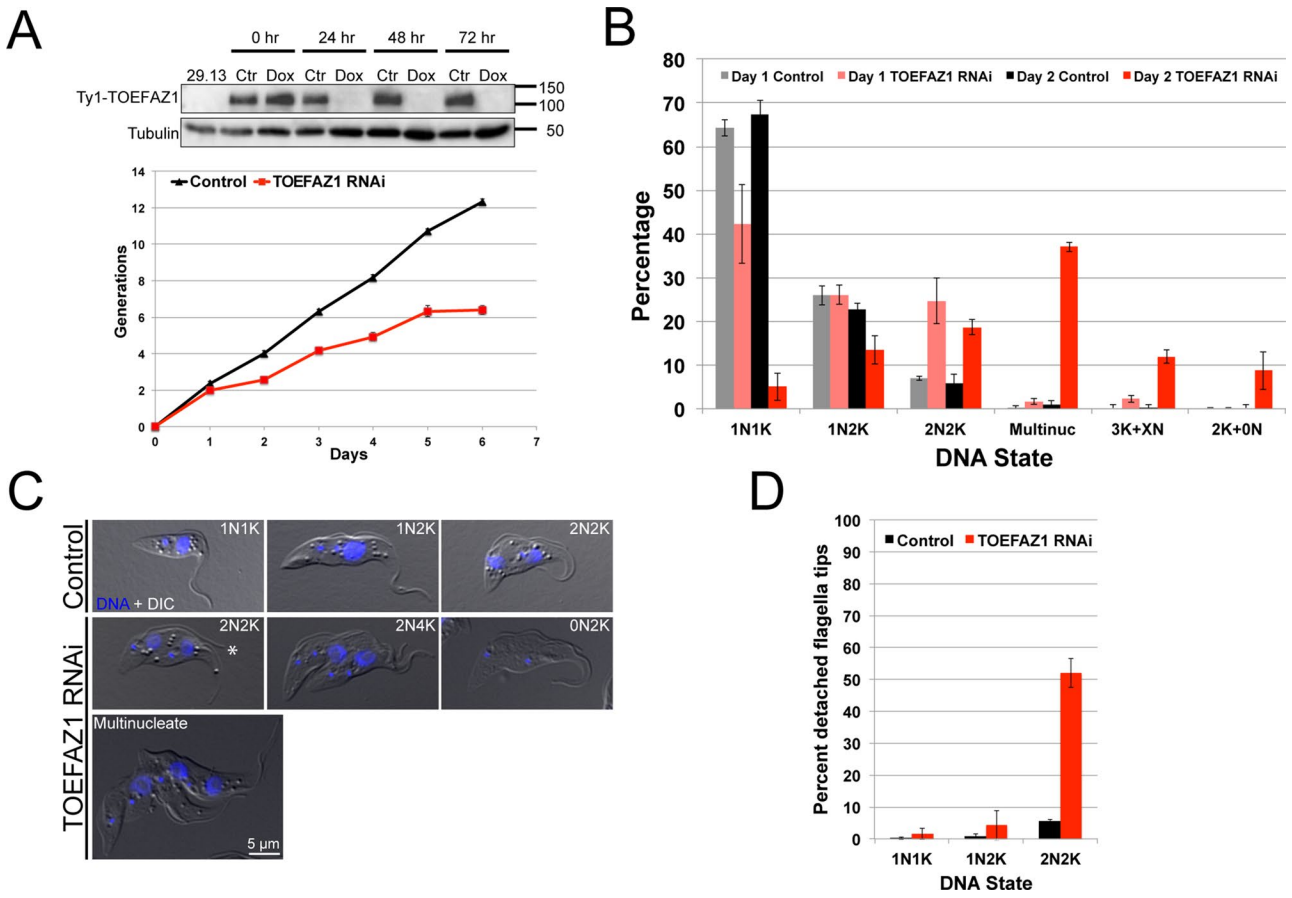

FIGURE 9: TOEFAZ1 depletion causes defects in cytokinesis. (A) TOEFAZ1 RNAi cells expressing 3X-Ty1-TOEFAZ1 from the endogenous locus were treated with doxycycline (DOX) or a vehicle control (Ctr). Cells were collected every 24 h to monitor TOEFAZ1 depletion by Ty1 Western blotting, using tubulin as a loading control. TOEFAZ1 RNAi cells were treated with doxycycline (TOEFAZ1 RNAi) or a vehicle control (Control), and the cell number was monitored over 6 d. (B) Quantitation of the DNA states of TOEFAZ1-depleted cells (TOEFAZ1 RNAi) and control cells (Control) after 1 d (gray, light red) or 2 d (black, red) of induction. 3K+XN, cells with three kinetoplasts and either one or two nuclei. 2K+0N, cells with two kinetoplasts and no nuclei. (C) Uninduced (Control) and cells depleted of TOEFAZ1 for 1 d (TOEFAZ1 RNAi) were treated with DAPI to label DNA (DNA; blue) and evaluated by fluorescence and DIC imaging. Asterisk shows detached new flagellum tip. (D) Quantitation of new flagellum tip detachment in cells depleted of TOEFAZ1 (TOEFAZ1 RNAi and Control cells).

FAZ. They are present at the location of the furrow and may also participate in positioning this structure. However, it should be noted that depletion of these proteins does not lead to an accumulation of 2N2K cells, as is the case with TOEFAZ1, although this may be due to their involvement in spindle pole formation. It is possible that the Aurora/CPC complex is recruited to the tip of the new FAZ to mark the completion of karyokinesis and signal that cytokinesis can proceed.

TOEFAZ1 depletion changes the distribution of TbPLK during the later stages of cell division. The kinase usually localizes to both the new FAZ tip and the FC as the new FAZ and flagellum are extending, but depleting TOEFAZ1 specifically blocks the recruitment of TbPLK to the new FAZ. This loss of localization is remarkably specific and has no effect on the FC-localized TbPLK. This suggests that TbPLK requires TOEFAZ1 to be recruited to the new FAZ, perhaps as a direct binding partner. TOEFAZ1 is a highly phosphorylated protein, and several of these sites fall within potential PLK-binding sites (Elia *et al.*, 2003; Snead *et al.*, 2007). The regulated TbPLK phosphosites are found in the TOEFAZ1 N-terminus, which is predicted to be a helical domain but lacks homology to any known structure. The function of these phosphosites may be important for loading TOEFAZ1 onto the tip of the new FAZ, although further work is necessary to establish the precise timing of the phosphorylation events, which might suggest other functions.

In this work, we have used a series of proteomic methods to identify candidate binding partners and substrates for TbPLK. This process is vital for moving from a descriptive understanding of TbPLK function, based strictly on observation of kinase migration and the consequences of kinase inhibition, to a more mechanistic understanding developed from establishing signaling circuits comprising kinase binding partners and substrates. Because TbPLK is involved in many essential processes throughout cell division, these circuits will be important for events such as FAZ and bilobe duplication, basal body rotation, and cytokinesis. A better understanding of the unique aspects of *T. brucei* cell division will uncover novel pathways for drug discovery, which is a vital concern.

MATERIALS AND METHODS

Cell culture

Experiments were performed in wild-type procyclic *T. brucei brucei* 427 strain and 427 cells carrying the machinery necessary for doxycycline inducibility (29-13). The 427 cells were cultured at 27°C in SDM-79 medium supplemented with 7.5 µg/ml hemin and 20%

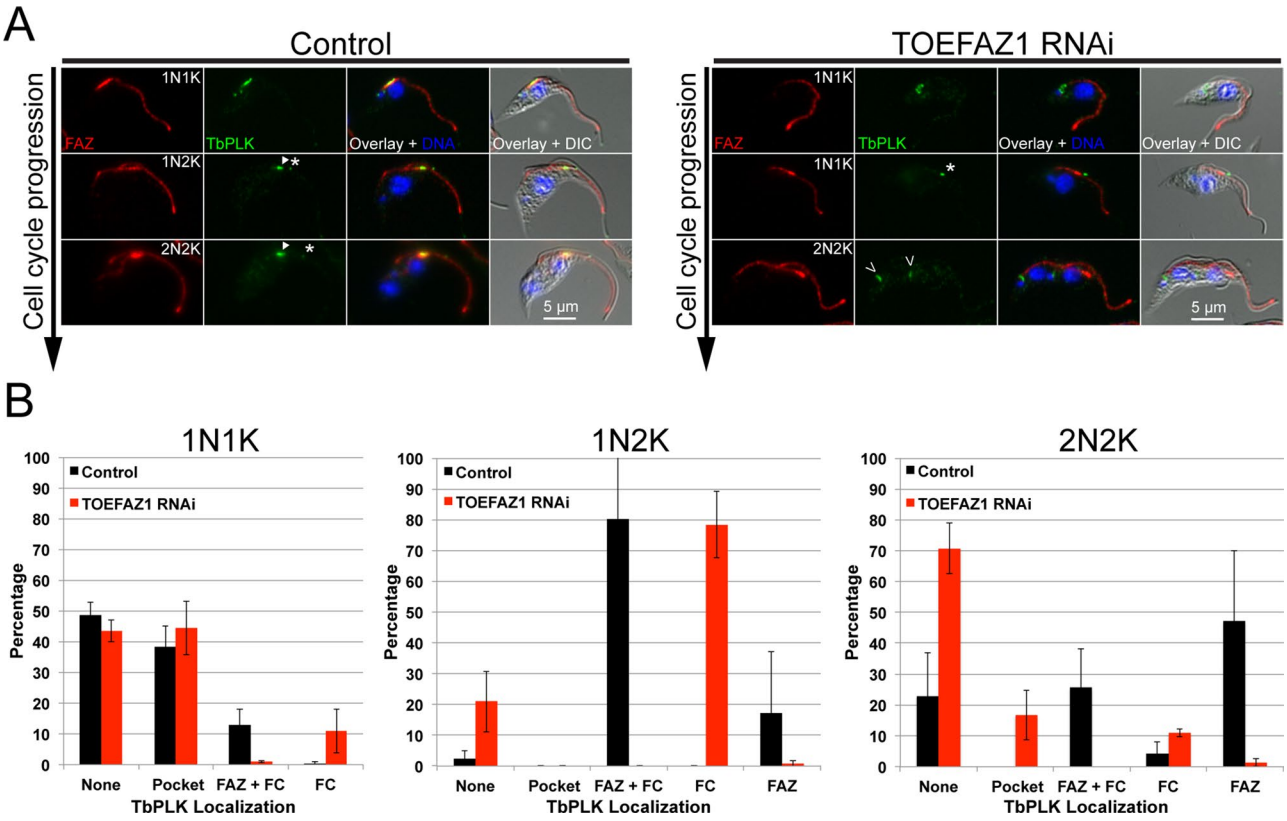

FIGURE 10: TOEFAZ1 depletion blocks recruitment of TbPLK to the tip of the new FAZ. (A) Control cells (Control) and cells depleted of TOEFAZ1 for 1 d (TOEFAZ1 RNAi) were fixed and labeled with an antibody against the FAZ (FAZ; red), antibodies against TbPLK (TbPLK; green), and DAPI to label the DNA (DNA; blue). Both samples were imaged using fluorescence and DIC microscopy. Filled arrowheads show the TbPLK labeling within the cell body, asterisks show TbPLK at the FC, and empty arrowheads show TbPLK that has been loaded onto the basal body region in 2N2K cells, which is aberrant. Rows show cells progressing through the cell cycle. (B) Quantitation of the localization of TbPLK in the control cells (Control) and TOEFAZ1-depleted (TOEFAZ1 RNAi) cells in A, sorted by DNA state.

fetal calf serum (Sigma-Aldrich, St. Louis, MO). The 29-13 cells were cultured at 27°C in SDM-79 medium supplemented with 7.5 µg/ml hemin, 20% doxycycline-free fetal calf serum (Clontech, Mountain View, CA), 50 µg/ml hygromycin, and 15 µg/ml neomycin. Cell growth was monitored using a particle counter (Z2 Coulter Counter, Beckman Coulter, Brea, CA; Moxi Z, Orflo, Ketchum, ID).

Antibodies

Antibodies were obtained from the following sources: anti-FAZ1 and AB1 from Keith Gull (Oxford University, Oxford, United Kingdom), anti–*Leishmania donovani* Centrin4 from Hira L. Nakhasi (U.S. Food and Drug Administration, Washington, DC), anti-Ty1 from Cynthia He (National University of Singapore, Singapore), 1B41 (Linda Kohl, Centre National de la Recherche Scientifique, Paris, France), anti-BILBO1 (Gang Dong, Max F. Perutz Laboratories, Vienna, Austria), 20H5 (Millipore Biosciences), and anti-TBBC (Etienne Pays, Université Libre de Bruxelles, Brussels, Belgium). The monoclonal antibodies against TbCentrin2 and TbCentrin4 and antibodies against TbPLK have been described previously (de Graffenried *et al.*, 2008; Ikeda and de Graffenried, 2012).

Cloning and cell line assembly

All DNA constructs were validated by sequencing. Verified constructs were introduced into cells using electroporation with a GenePulser Xcell (Bio-Rad, Hercules, CA), and clonal cell lines were generated by selection and limiting dilution.

The myc-BirA*-TbPLK construct was assembled in the vector pLEW100 by cloning myc-BirA* into a pLEW100 variant that already contained the TbPLK open reading frame using the restriction enzymes *Hin*dIII and *Bam*HI, which installed the biotinylation machinery at the N-terminus of the kinase. Myc-BirA* was previously used in *T. brucei* (Morriswood *et al.*, 2013). The completed plasmid was linearized with *Not*I, and clonal lines were selected with 5 µg/ml phleomycin.

Endogenous tagging with a triple-Ty1 tag was accomplished using previously described methods (Morriswood *et al.*, 2009). Targeting the tag to the N-terminus of the endogenous locus of each candidate protein was mediated by 500 base pairs of 5′ untranslated region sequence and the first 500 base pairs of the open reading frame. The targeting constructs were assembled in a sequencing plasmid (PCR4Blunt) and then excised by restriction digest before electroporation into 427 cells. Clonal lines were selected with 20 µg/ml blasticidin. Presumed clones were screened for correct recombination at the endogenous locus by PCR using genomic DNA, followed by Ty1 Western blotting and immunofluorescence microscopy.

Doxycycline-inducible RNAi stem-loops were assembled in pTrypRNAiGate using previously published methods (Kalidas *et al.*, 2011). Targeting sequences were chosen using the RNAit software (trypanofan.bioc.cam.ac.uk/software/RNAit.html). The specific gene segments are as follows: TOEFAZ1, nucleotides (nt) 578–1090; FC1, nt 1265–1763; and FAZ9, nt 1511–1687. The completed RNAi constructs were then linearized using the

restriction enzyme *Not*I and electroporated into the 29-13 cell line (Wirtz *et al.*, 1999). Stable transformants were selected with 20 µg/ml Zeocin (Invitrogen, Carlsbad, CA), and clonal cell lines were generated by limiting dilution. Endogenous replacement of TOEFAZ1, FC1, and FAZ9 in the 29-13 cell lines carrying the complementary RNAi construct with the Ty1 epitope at the N-terminus was accomplished as described.

RNAi

Cultures of TOEFAZ1, FC1, or FAZ9 RNAi cells were seeded at 1×10^6 cells/ml and induced by adding 1 µg/ml doxycycline, and 70% ethanol was added to control cells. Cells were maintained at 27°C and reseeded every 48 h with fresh medium and doxycycline. Cells were counted every 24 h and samples taken for Western blot analysis and immunofluorescence microscopy. All cell counts are the average of three biological replicates, and the error bars are the SE. For quantitation by microscopy, FC1 was depleted for 2 d, TOEFAZ1 for 1 d, and FAZ9 for 4 d, unless otherwise noted.

Scanning electron microscopy

EM-grade glutaraldehyde (TAAB, Reading, United Kingdom) was added directly to the suspension culture flask directly from the incubator to a final concentration of 2.5% EM-grade glutaraldehyde. The fixed cell suspension was then resuspended in primary fixative of 2.5% EM-grade glutaraldehyde in phosphate-buffered saline (PBS) for 2 h at room temperature on a rocking stage. Cells were washed twice with PBS and settled onto 13-mm round glass coverslips. Once adhered, the coverslips were washed with double-distilled dH_2O to remove any buffer. Dehydration steps were 30, 50, 70, and 90% ethanol in H_2O added sequentially to the coverslips for 5 min each, followed by 3×5 min in 100% ethanol. Finally, the samples were dried using a critical point dryer and coated with gold using a sputter coater. Images were taken on a Hitachi S-3400N.

BioID

The myc-BirA*-TbPLK cell line was seeded in medium supplemented with 50 µM biotin for 24 h before induction. Two 500-ml cultures were seeded at 4×10^6 cells/ml and then induced for 18 h with either 20 ng/ml doxycycline to initiate expression of myc-BirA*-TbPLK or a vehicle control (70% ethanol). The cells were harvested by centrifugation, and biotinylated proteins were isolated on streptavidin beads as described previously (Roux *et al.*, 2012; Morriswood *et al.*, 2013). For the BioID conducted on soluble and pellet fractions, the harvested cell pellets were resuspended in PEME buffer (2 mM ethylene glycol tetraacetic acid [EGTA], 1 mM $MgSO_4$, 0.1 mM EDTA, 0.1 M 1,4-piperazinediethanesulfonic acid [PIPES], pH 6.9) supplemented with 0.5% NP-40 and a cOmplete (Roche) protease inhibitor pellet for 5 min at room temperature. The samples were then centrifuged at $14,000 \times g$ for 10 min at room temperature. The supernatant fraction was separated from the pellet, and biotinylated proteins were isolated as described. The pellet fractions were washed once with PEME plus 0.25% NP-40 and then resuspended in BioID lysis buffer (0.4% SDS, 2% Triton X-100, 500 mM NaCl, 5 mM EDTA, 1 mM dithiothreitol [DTT], 50 mM Tris, pH 7.4) followed by isolation of biotinylated proteins.

Immunofluorescence

Cells were harvested, washed once in PBS, and then adhered to coverslips. For DNA and DIC analysis, cells were fixed in 4% paraformaldehyde in PBS for 20 min at room temperature, followed by three washes in PBS before mounting. For direct methanol fixation, the cells were immersed in –20°C methanol for 20 min, air dried, and then rehydrated in PBS. For extracted cytoskeletons, the cells on coverslips were incubated in extraction buffer (0.1 M PIPES, pH 6.9, 2 mM EGTA, 1 mM $MgSO_4$, 0.1 mM EDTA, 1% NP-40) for 5 min at room temperature, washed in PBS three times, followed by fixation in –20°C methanol for 20 min and rehydration in PBS. The cells were blocked overnight at 4°C in blocking buffer (PBS containing 3% bovine serum albumin). Primary antibodies were diluted in blocking buffer and incubated for 1 h at room temperature and then washed four times in PBS and placed in blocking buffer for 20 min. Alexa 488– or 568–conjugated secondary antibodies (Life Technologies, Carlsbad, CA) were diluted in blocking buffer and incubated for 1 h at room temperature. Cells were washed and mounted in Fluoromount G with DAPI (Southern Biotech, Birmingham, AL). Coverslips were imaged using a Zeiss Observer Z1 equipped with a CoolSNAP HQ2 camera (Photometrics, Tucson, AZ) and a Plan-Apochromat 63×/1.4 oil immersion lens (Zeiss, Thornwood, NY). AxioVision, release 4.8, was used to control the microscope for acquisition. All images were quantified in ImageJ (National Institutes of Health, Bethesda, MD) and assembled for publication using Photoshop CS5 and Illustrator CS5.

Western/streptavidin blotting

Cells were harvested, washed once in PBS, and then lysed in SDS–PAGE loading buffer. A total of 3×10^6 cell equivalents of lysate/lane was fractionated using SDS–PAGE, transferred to nitrocellulose, and blocked for 1 h at room temperature. For antibody detection, blocking and antibody dilution were done in Tris-buffered saline (TBS) supplemented with 5% nonfat milk and 0.1% Tween-20. Primary antibodies were incubated overnight at 4°C, followed by washing in TBS containing 0.1% Tween-20 and incubation with secondary antibodies conjugated to horseradish peroxidase (HRP; Jackson ImmunoResearch, West Grove, PA). For streptavidin blotting, membranes were blocked in 10% milk and 0.3% Tween-20 in PBS and then incubated with HRP-conjugated streptavidin (Life Technologies) overnight at 4°C. The blots were then washed in PBS/0.3% Tween-20. Clarity (Bio-Rad) ECL substrate and a Bio-Rad Gel Doc XR+ documentation system were used for detection.

Measurements

FAZ length measurements were conducted using the freehand drawing tool in ImageJ (1.49J). Before measurement, black and white maximum intensity *Z*-projections of the FAZ channel were generated to ensure that the full length of the structure was evident. The DNA channel was used to select 1N1K cells. The measurements were exported to Excel for analysis.

Statistics

All error bars represent the SD from the mean for three biological replicates. For DNA counting and phenotype quantitation by microscopy, at least 250 cells were counted for the RNAi and control conditions for each biological replicate. For FAZ measurements, 100 FAZs from 1N1K cells for the RNAi and control conditions were selected for each biological replicate.

SILAC experiments

For the SILAC experiments, cells were grown in SDM-79 lacking arginine and lysine (Caisson Labs, North Logan, UT) supplemented with 20% dialyzed serum (Invitrogen). The medium was further supplemented with either isotopically labeled 126 µg/ml arginine ($^{13}C_6$, 99%; $^{15}N_4$, 99%; Cambridge Isotope Laboratories, Tewksbury, MA) and 75 µg/ml lysine ($^{13}C_6$, 99%; Cambridge Isotope Laboratories) or unlabeled amino acids. Cells with and without the isotopically

labeled amino acids were grown for six cell cycles to allow for full incorporation, which was confirmed by LC-MS/MS of the labeled sample. Growth of both cultures was monitored to ensure that there was no difference in cell proliferation. Cultures containing 3.1×10^8 cells each were seeded at 2.5×10^6 cells/ml. The light sample was treated with 5 μM 3MB-PP1 for 2 h, and the heavy sample was treated with DMSO as a vehicle control. The samples were incubated at 27°C for 2 h, at which point the cells were pelleted, combined, and washed once with serum-free SDM-79 lacking Arg and Lys. The combined pellet was then lysed in modified RIPA buffer (50 mM Tris, pH 7.4, 150 mM NaCl, 2 mM EDTA, 1% NP-40, 0.1% SDS) containing 3 M urea and one tablet each of phosSTOP phosphatase inhibitors (Roche, Branford, CT) and cOmplete mini protease inhibitors per 5 ml of lysis buffer. The sample was centrifuged at 10,000 × *g* at 4°C for 10 min, and then the supernatant was processed for phosphoproteomic analysis.

Double-cut elutriation/iTRAQ

Double-cut elutriation on TbPLK analogue–sensitive cells was performed as previously described (Lozano-Núñez *et al.*, 2013). Briefly, ~4×10^9 cells were collected for double-cut elutriation, which was performed as previously described (Archer *et al.*, 2011), except for the interval between the first and second cuts, which was extended to 90 min. Equal quantities of synchronous cells were split into two cultures and allowed to progress through the cell cycle for 90 min, when 5 μM 3MB-PP1 was added to one culture and a vehicle control (DMSO) was added to the other. The two cultures were incubated at 27°C for 1 h, then washed and lysed in modified RIPA buffer as performed in the SILAC experiments.

BioID sample processing and LC-MS/MS

Samples were processed and analyzed essentially as previously described (Morriswood *et al.*, 2013). Beads were washed with 50 mM ammonium bicarbonate, disulfide bridges were reduced with DTT, and thiols were alkylated with iodoacetamide. Proteins were digested on bead with trypsin (recombinant, proteomics grade; Roche) overnight at 37°C. Acidified peptides were separated on an UltiMate 3000 nanoHPLC or an UltiMate 3000 nanoRSLC applying a 90-min linear gradient from 2 to 32% acetonitrile (ACN) on a C18 analytical column.

The high-performance liquid chromatograph (HPLC) was directly coupled to an LTQ-Orbitrap Velos mass spectrometer via a nano electrospray ionization source. The electrospray voltage was set to 1.5 kV. The mass spectrometer was operated in the data-dependent mode: one full scan (m/z = 350–1800, resolution 60,000) was followed by maximal 20 MS/MS scans. The lock mass was enabled and set at the signal of polydimethylcyclosiloxane at m/z = 445.120025. Monoisotopic precursor selection was enabled, and singly charged signals were excluded from fragmentation. The collision energy was set at 35%, *Q*-value at 0.25, and activation time at 10 ms.

Data interpretation

Raw spectra were interpreted by Mascot 2.2.04 (Matrix Science, Boston, MA) using Mascot Daemon 2.2.2. Spectra were searched against the TriTryp database of Tbrucei427 and Tbrucei927 (18,355 entries, 23-apr-2012, tritrypdb.org/), including common contaminants. The following search parameters were used: peptide tolerance was set to 2 ppm, MS/MS tolerance to 0.8 Da, trypsin was selected as protease and two missed cleavages were allowed, and carbamidomethyl cysteine was set as static modification and oxidation of methionine as a variable modification. MASCOT results were loaded into Scaffold (version 3.00.02; Proteome Software, Portland, OR). Peptide identifications were accepted if a probability >95% was assigned by the Protein Prophet algorithm. Protein identifications were accepted if they could be established at a probability >99%. A list of potential specific TbPLK interaction partners was generated taking into account the spectral counts in the induced and noninduced samples and the occurrence in biological replicates.

All mass spectrometers used, including electrospray ionization source, and HPLC systems, including columns, were from Thermo Fisher Scientific/Dionex if not otherwise specified.

Trypsinization and peptide isolation for phosphoproteomics

Crude cell extracts were digested to peptides in a filtration device, a method termed filter-aided sample preparation (FASP). For the iTRAQ samples, the FASP protocol was used essentially as described (Wiśniewski *et al.*, 2009). Cell lysates were sonicated for 5 min and then mixed with 3 ml UA (8 M urea, 50 mM triethylammonium bicarbonate [TEAB], pH 8). This solution was loaded onto an Amicon Ultra-4 centrifugal filter unit with a 30-kDa MWCO (UFC 903024; Millipore, Billerica, MA). Filter units were centrifuged at 4000 × *g* at room temperature until the retentate was reduced to 1/10 of the starting volume. The retenate was washed two times with UA with subsequent centrifuging. For reduction of the disulfide bridges, the sample was incubated with 1 μg of Tris(2-carboxyehtyl) phosphine/2.5 μg of protein for 1 h at 60°C. Then the thiol groups were alkylated by adding 17 μl of 200 mM methyl methanesulfonothioate (MMTS; 1 μg/2.5 μg of protein) and incubating for 30 min in the dark. The filter units were then washed twice with UA and then twice with 3 ml of 0.8 M urea and 50 mM TEAB, pH 8. Proteins were digested with trypsin (1 μg/30–50 μg of protein) at 37°C overnight with gentle shaking. Liquid that passed through the filter was combined with the retenate, and trypsin at a ratio of 1 μg of trypsin/200 μg of protein was added and incubated for another 2–4 h for completing the digest. Filter tubes were centrifuged (4000 × *g* at room temperature) until void volume was reached and then washed twice with 200 μl of 50 mM TEAB, pH 8 (5-min incubation). The filtrates were pooled and lyophilized to dryness.

The SILAC samples were processed with the following exceptions: sonicated cell extracts were loaded onto an Amicon Ultra-15 centrifugal filter. Protocol was performed with 10 ml of 8 M urea and 50 mM ammonium bicarbonate (ABC) instead of UA. Washing steps were preceded by 10 ml of 8 M urea plus 50 mM ABC and 0.8 M urea plus 50 mM ABC, respectively. Disulfide groups were reduced with DTT (1 μg of DTT/20 μg of protein) for 30 min at 56°C and subsequently alkylated with iodoacetamide (IAA; 1 μg of IAA/4 μg of protein) for 20 min in the dark.

iTRAQ labeling

Peptides were labeled with iTRAQ (ABSciex, Redwood City, CA) according to the manufacturer's instructions. Each dried sample was dissolved in 100 μl of 500 mM TEAB, pH 8, and labeled for 2.5 h at room temperature with 1 U of labeling reagent diluted in 70 μl of ethanol/250 μg of peptide. Labeling efficiency was tested in an LC-MS/MS run at the PSM level and found to be >98% for all labels. For confident quantification ratios, we performed duplicate duplex experiments: each sample was split, and each half was labeled with a different iTRAQ reagent (either labels 114 and 115 or labels 116 and 117 were combined). The four channels were mixed at a 1:1:1:1 ratio (mixing deviation was defined in an LC-MS run and found to be <10%) and desalted with Strata-X SPE cartridges (Phenomenex, Torrance, CA) and lyophilized.

Desalting was performed with Strata-X SPE cartridges (Phenomenex) conditioned with 70% ACN, 0.1% formic acid [FA],

followed by equilibration with 0.1% trifluoroacetic acid [TFA]. After sample loading, washing was performed with 0.1% TFA, followed by 0.1% FA, and then elution with 70% ACN, 0.1% FA). In some cases SEP-PAK tC18 cartridges (Waters) or Empore C18 SD (3M) were employed. These cartridges were washed with 100% MeOH, conditioned with 70% ACN and 0.1% FA, and then equilibrated with 0.1% TFA. After sample loading, they were washed with 0.1% TFA, followed by 0.1% FA, and then eluted with 70% ACN and 0.1% FA. Eluates were lyophilized.

Phosphopeptide enrichment

Phosphopeptide enrichment was essentially performed as described previously (Bodenmiller *et al.*, 2007). Peptides of 1.7 mg of digested protein were reconstituted in 280 µl of solution of 80% ACN and 3.5% TFA saturated with phthalic acid. The peptides were added to 850 µg of TiO_2 spheres (GL Sciences, Tokyo, Japan) equilibrated with the saturated phthalic acid solution and incubated in a Mobicol spin column (MoBiTec, Goettingen, Germany) for 30 min while rotating. The column was washed two times with 200 µl of saturated phthalic acid solution, two times with 300 µl of 80% ACN and 0.1% TFA, and finally two times with 300 µl of 1%ACN and 0.1% TFA. The bound peptides were eluted with two times with 150 µl of 0.3 M NH_4OH solution. The eluates were combined and acidified immediately with 5 µl of concentrated TFA.

iTRAQ strong cation exchange

Fractionation of phosphopeptides by strong cation exchange (SCX) tips (Glygen; Top Tip PolySULFOETHYL A; Columbia, MD) was performed following an adapted protocol: washing with 2 × 30 µl of 30% ACN, 2 × 30 µl of 80% ACN, 2 × 30 µl of H_2O; conditioning with 30 µl of 5 mM $NaPO_4$, pH 2.7, 15% ACN, and 500 mM NaCl. Tips were equilibrated with 10 times 30 µl of 5 mM $NaPO_4$, pH 2.7, and 15% ACN. Desalted and freeze-dried peptide samples were dissolved in 30 µl of 5 mM $NaPO_4$, pH 2.7, and 15%ACN, loaded slowly onto the tips, and washed with 20 µl of 5 mM Na-PO_4, pH 2.7, and 15% ACN. Bound peptides were eluted by a six-step elution with increasing salt concentration (20, 30, 40, 60, 100, 300 mM NaCl; 30-µl fraction volume). Fractions were reduced to a volume of 5 µl in a SpeedVac in order to evaporate ACN and then filled up to a final volume of 50 µl with 0.1% TFA.

iTRAQ LC-MS/MS

Peptides were separated on a U3000 nano RSLC system. Each fraction was loaded on a trapping column (PepMap C18, 5-µm particle size, 300-µm inner diameter × 5 mm) equilibrated with 0.1% TFA and separated on an analytical column (PepMap C18, 3 µm, 75-µm inner diameter × 150 mm) by applying a 180-min linear gradient from 1.6 to 32% ACN with 0.1% formic acid followed by a washing step with 80% ACN. The nano-HPLC was directly coupled to the LTQ-Orbitrap Velos hybrid mass spectrometer via the electrospray ionization source. The mass spectrometer was operated in the data-dependent mode: one full scan (m/z = 350–2000, resolution 60,000) was followed by alternate fragmentation of the top five precursors with higher-energy collisional dissociation (HCD) and collision-induced dissociation (CID). For internal calibration, the lock mass was set at the signal of polydimethylcyclosiloxane at m/z = 445.120025. Monoisotopic precursor selection was enabled; precursors with charge state 1 were excluded from fragmentation. The collision energy for CID was set at 35%, *Q*-value at 0.25, and activation time at 10 ms. For HCD, the collision energy was set at 45% and activation time at 0.1 ms. Fragmented ions were excluded from further fragmentation for 60 s.

iTRAQ data analysis

Raw files were processed with the Proteome Discoverer 1.4.0.288 (Thermo Fisher Scientific, Waltham, MA). Spectra were searched with the following parameters with Mascot (Matrix Science): proteolytic specificity of trypsin allowing two missed cleavages, MMTS alkylation of cysteines as fixed modification, oxidation of Met, phosphorylation of Ser, Thr, and Tyr, and labeling of the N-terminus of peptides and of Lys and Tyr with iTRAQ as variable modification. Precursor tolerance was set to 10 ppm and fragment tolerance for CID spectra to 0.8 Da and for HCD spectra to 20 mDa.

Quantitative data in the HCD scans were interpreted with the reporter ion quantitation node in the Proteome Discoverer with an integration tolerance of 20 mDa. Results were filtered for complete iTRAQ labeling of the peptides. Unbalanced mixing of the four channels was corrected based on the ratio of the duplicated channels; quantification data with one channel missing were not considered. The phosphorylated peptides exhibiting an inhibitor dependence (ratio >2 or <0.5) were manually inspected regarding identity and quantitation.

SILAC SCX separation

Phosphopeptides were further fractionated on an UltiMate Plus nano HPLC equipped with a SCX column from PolyLC (PolySULFOETHYL A, 100 × 2.1 mm, 3 µm, 100 Å). The lyophilized samples were dissolved in 60 µl of 5 mM Na-PO_4, pH 2.7, buffer with 15% ACN and loaded on the SCX column. A 60-min linear gradient was applied from 0 to 500 mM NaCl in 5 mM $NaPO_4$, pH 2.7, buffer with 15% ACN at a flow rate of 30 µl/min. One-minute fractions were collected over 100 min and pooled depending on their peptide content before the LC-MS measurement.

SILAC LC-MS/MS

The desalted SCX-fractions from the SILAC experiments were separated on an UltiMate 3000 nanoRSLC essentially as described for the iTRAQ samples. After the samples were preconcentrated on a C18 reversed-phase trap column, the peptides were separated on a C18 reversed-phase analytical column, applying a 60-min linear gradient from 1.6 to 32% ACN with 0.08% FA at a flow rate of 275 nl/min. The HPLC was coupled to an LTQ Orbitrap Velos mass spectrometer via a nano-electrospray ionization source. The mass spectrometer was operated in a data-dependent mode: one full scan in the Orbitrap (m/z = 350–2000, 60,000 resolution) was followed by MSMS scans in the linear ion trap of the 12 most intense precursor ions (35% collision energy; *Q*-value 0.25; activation time 10 ms). Internal calibration with lock mass (m/z = 445.120024, polydimethylcyclosiloxane) was enabled. Precursors with charge state 1 were excluded for fragmentation. Monoisotopic precursor selection was enabled. Fragmented ions were put on an exclusion list for 30 s.

The first SILAC experiment was measured on a QExactive: one full scan in the Orbitrap (m/z = 350–2000, 70,000 resolution) was followed by HCD fragmentation of the 10 most intense precursor ions (30% normalized collision energy). During manual validation, we observed jagged peaks in the extracted ion chromatograms, which led to false quantitation ratios especially when signals were low. Therefore the following SILAC experiments were all measured on an LTQ Orbitrap Velos.

SILAC data analysis

SILAC data were interpreted with MaxQuant 1.5.0. Raw data were searched against the TriTryp database with tryptic specificity allowing a maximum of two missed cleavages. Oxidation of methionine and phosphorylation of serine, threonine, and tyrosine were set as

variable and carbamidomethylation of cysteines as fixed modification. Lys-6 and Arg-10 were defined as heavy labels. A minimum peptide length of 7 was required. Precursor tolerance was set to 4.5 ppm and fragment tolerance to 0.5 Da. Results were filtered for 1% false discovery rate at the peptide level.

The phosphorylated peptides exhibiting an inhibitor dependence (ratio >2 or <0.5) were manually inspected regarding identity and quantitation.

ACKNOWLEDGMENTS

We thank Gustav Ammerer for advice on mass spectrometry, Graham Warren and the Warren lab for support, Richard Bennett for the use of his microscope, and all of the labs that provided essential reagents. We also thank Samantha Barry (Oxford Brookes University) for support and help with electron microscopy. This work was supported by startup funds from Brown University, the Austrian Science Fund (Grant P21550-B12, Doctoral Program Molecular Mechanisms of Cell Signaling W1220-B09), and the National Institutes of Health (NIGMS P20 GM104317, NIAID R01AI112953). This article is dedicated to the memory of Elisabetta Ullu.

REFERENCES

Aksoy S, Caccone A, Galvani AP, Okedi LM (2013). Glossina fuscipes populations provide insights for human African trypanosomiasis transmission in Uganda. Trends Parasitol 29, 394–406.

André J, Harrison S, Towers K, Qi X, Vaughan S, McKean PG, Ginger ML (2013). The tubulin cofactor C family member TBCCD1 orchestrates cytoskeletal filament formation. J Cell Sci 126, 5350–5356.

Archambault V, Glover DM (2009). Polo-like kinases: conservation and divergence in their functions and regulation. Nat Rev Mol Cell Biol 10, 265–275.

Archer SK, Inchaustegui D, Queiroz R, Clayton C (2011). The cell cycle regulated transcriptome of Trypanosoma brucei. PLoS One 6, e18425.

Bashor CJ, Helman NC, Yan S, Lim WA (2008). Using engineered scaffold interactions to reshape MAP kinase pathway signaling dynamics. Science 319, 1539–1543.

Bastin P, Bagherzadeh Z, Matthews KR, Gull K (1996). A novel epitope tag system to study protein targeting and organelle biogenesis in Trypanosoma brucei. Mol Biochem Parasitol 77, 235–239.

Bastos RN, Barr FA (2010). Plk1 negatively regulates Cep55 recruitment to the midbody to ensure orderly abscission. J Cell Biol 191, 751–760.

Bishop AC *et al*. (2000). A chemical switch for inhibitor-sensitive alleles of any protein kinase. Nature 407, 395–401.

Bodenmiller B, Mueller LN, Mueller M, Domon B, Aebersold R (2007). Reproducible isolation of distinct, overlapping segments of the phosphoproteome. Nat Methods 4, 231–237.

Bonhivers M, Nowacki S, Landrein N, Robinson DR (2008). Biogenesis of the trypanosome endo-exocytotic organelle is cytoskeleton mediated. PLoS Biol 6, e105.

Briggs LJ, McKean PG, Baines A, Moreira-Leite F, Davidge J, Vaughan S, Gull K (2004). The flagella connector of Trypanosoma brucei: an unusual mobile transmembrane junction. J Cell Sci 117, 1641–1651.

Brun R, Blum J, Chappuis F, Burri C (2010). Human African trypanosomiasis. Lancet 375, 148–159.

Burkard ME, Randall CL, Larochelle S, Zhang C, Shokat KM, Fisher RP, Jallepalli PV (2007). Chemical genetics reveals the requirement for Polo-like kinase 1 activity in positioning RhoA and triggering cytokinesis in human cells. Proc Natl Acad Sci USA 104, 4383–4388.

Chanez A-L, Hehl AB, Engstler M, Schneider A (2006). Ablation of the single dynamin of T. brucei blocks mitochondrial fission and endocytosis and leads to a precise cytokinesis arrest. J Cell Sci 119, 2968–2974.

Davidge JA, Chambers E, Dickinson HA, Towers K, Ginger ML, McKean PG, Gull K (2006). Trypanosome IFT mutants provide insight into the motor location for mobility of the flagella connector and flagellar membrane formation. J Cell Sci 119, 3935–3943.

de Graffenried CL, Anrather D, Von Raussendorf F, Warren G (2013). Polo-like kinase phosphorylation of bilobe-resident TbCentrin2 facilitates flagellar inheritance in Trypanosoma brucei. Mol Biol Cell 24, 1947–1963.

de Graffenried CL, Ho HH, Warren G (2008). Polo-like kinase is required for Golgi and bilobe biogenesis in Trypanosoma brucei. J Cell Biol 181, 431–438.

Dou Z, Schubert von C, Körner R, Santamaria A, Elowe S, Nigg EA (2011). Quantitative mass spectrometry analysis reveals similar substrate consensus motif for human Mps1 kinase and Plk1. PLoS One 6, e18793.

DuBois KN, Alsford S, Holden JM, Buisson J, Swiderski M, Bart J-M, Ratushny AV, Wan Y, Bastin P, Barry JD, *et al*. (2012). NUP-1 Is a large coiled-coil nucleoskeletal protein in trypanosomes with lamin-like functions. PLoS Biol 10, e1001287.

Elia AEH, Cantley LC, Yaffe MB (2003). Proteomic screen finds pSer/pThr-binding domain localizing Plk1 to mitotic substrates. Science 299, 1228–1231.

Engstler M, Pfohl T, Herminghaus S, Boshart M, Wiegertjes G, Heddergott N, Overath P (2007). Hydrodynamic flow-mediated protein sorting on the cell surface of trypanosomes. Cell 131, 505–515.

Esson HJ, Morriswood B, Yavuz S, Vidilaseris K, Dong G, Warren G (2012). Morphology of the Trypanosome bilobe, a novel cytoskeletal structure. Eukaryot Cell 11, 761–772.

Farr H, Gull K (2012). Cytokinesis in trypanosomes. Cytoskeleton (Hoboken) 69, 931–941.

Fèvre EM, Wissmann BV, Welburn SC, Lutumba P (2008). The burden of human African trypanosomiasis. PLoS Negl Trop Dis 2, e333.

Field MC, Carrington M (2009). The trypanosome flagellar pocket. Nat Rev Microbiol 7, 775–786.

Gadelha C, Rothery S, Morphew M, McIntosh JR, Severs NJ, Gull K (2009). Membrane domains and flagellar pocket boundaries are influenced by the cytoskeleton in African trypanosomes. Proc Natl Acad Sci USA 106, 17425–17430.

Gallet C, Demonchy R, Koppel C, Grellier P, Kohl L (2013). A protein phosphatase 1 involved in correct nucleus positioning in trypanosomes. Mol Biochem Parasitol 192, 49–54.

Gallo JM, Précigout E, Schrével J (1988). Subcellular sequestration of an antigenically unique beta-tubulin. Cell Motil Cytoskeleton 9, 175–183.

Gheiratmand L, Brasseur A, Zhou Q, He CY (2013). Biochemical characterization of the bi-lobe reveals a continuous structural network linking the bi-lobe to other single-copied organelles in Trypanosoma brucei. J Biol Chem 288, 3489–3499.

Gull K (1999). The cytoskeleton of trypanosomatid parasites. Annu Rev Microbiol 53, 629–655.

Gull K (2003). Host-parasite interactions and trypanosome morphogenesis: a flagellar pocketful of goodies. Curr Opin Microbiol 6, 365–370.

Hammarton TC, Clark J, Douglas F, Boshart M, Mottram JC (2003). Stage-specific differences in cell cycle control in Trypanosoma brucei revealed by RNA interference of a mitotic cyclin. J Biol Chem 278, 22877–22886.

Hammarton TC, Kramer S, Tetley L, Boshart M, Mottram JC (2007a). Trypanosoma brucei Polo-like kinase is essential for basal body duplication, kDNA segregation and cytokinesis. Mol Microbiol 65, 1229–1248.

Hammarton TC, Monnerat S, Mottram JC (2007b). Cytokinesis in trypanosomatids. Curr Opin Microbiol 10, 520–527.

Hayes P, Varga V, Olego-Fernandez S, Sunter J, Ginger ML, Gull K (2014). Modulation of a cytoskeletal calpain-like protein induces major transitions in trypanosome morphology. J Cell Biol 206, 377–384.

He CY, Pypaert M, Warren G (2005). Golgi duplication in Trypanosoma brucei requires Centrin2. Science 310, 1196–1198.

Hoare CA, Wallace FG (1966). Developmental stages of trypanosomatid flagellates: a new terminology. Nature 212, 1385–1386.

Huber AH, Nelson WJ, Weis WI (1997). Three-dimensional structure of the armadillo repeat region of beta-catenin. Cell 90, 871–882.

Hughes L, Towers K, Starborg T, Gull K, Vaughan S (2013). A cell-body groove housing the new flagellum tip suggests an adaptation of cellular morphogenesis for parasitism in the bloodstream form of Trypanosoma brucei. J Cell Sci 126, 5748–5757.

Ikeda KN, de Graffenried CL (2012). Polo-like kinase is necessary for flagellum inheritance in Trypanosoma brucei. J Cell Sci 125, 3173–3184.

Johnson EF, Stewart KD, Woods KW, Giranda VL, Luo Y (2007). Pharmacological and functional comparison of the polo-like kinase family: insight into inhibitor and substrate specificity. Biochemistry 46, 9551–9563.

Kalidas S, Li Q, Phillips MA (2011). A Gateway® compatible vector for gene silencing in bloodstream form Trypanosoma brucei. Mol Biochem Parasitol 178, 51–55.

Kean MJ, Couzens AL, Gingras A-C (2012). Mass spectrometry approaches to study mammalian kinase and phosphatase associated proteins. Methods 57, 400–408.

Kee HL, Dishinger JF, Blasius TL, Liu C-J, Ben Margolis, Verhey KJ (2012). A size-exclusion permeability barrier and nucleoporins characterize a ciliary pore complex that regulates transport into cilia. Nat Cell Biol 14, 431–437.

Kohl L, Sherwin T, Gull K (1999). Assembly of the paraflagellar rod and the flagellum attachment zone complex during the Trypanosoma brucei cell cycle. J Eukaryot Microbiol 46, 105–109.

Kumar P, Wang CC (2006). Dissociation of cytokinesis initiation from mitotic control in a eukaryote. Eukaryot Cell 5, 92–102.
Lacomble S, Vaughan S, Gadelha C, Morphew MK, Shaw MK, McIntosh JR, Gull K (2009). Three-dimensional cellular architecture of the flagellar pocket and associated cytoskeleton in trypanosomes revealed by electron microscope tomography. J Cell Sci 122, 1081–1090.
Lacomble S, Vaughan S, Gadelha C, Morphew MK, Shaw MK, McIntosh JR, Gull K (2010). Basal body movements orchestrate membrane organelle division and cell morphogenesis in Trypanosoma brucei. J Cell Sci 123, 2884–2891.
LaCount DJ, Barrett B, Donelson JE (2002). Trypanosoma brucei FLA1 is required for flagellum attachment and cytokinesis. J Biol Chem 277, 17580–17588.
Langousis G, Hill KL (2014). Motility and more: the flagellum of Trypanosoma brucei. Nat Rev Microbiol 12, 505–518.
Li Z, Lee JH, Chu F, Burlingame AL, Günzl A, Wang CC (2008a). Identification of a novel chromosomal passenger complex and its unique localization during cytokinesis in Trypanosoma brucei. PLoS One 3, e2354.
Li Z, Umeyama T, Wang CC (2008b). The chromosomal passenger complex and a mitotic kinesin interact with the Tousled-like kinase in trypanosomes to regulate mitosis and cytokinesis. PLoS One 3, e3814.
Li Z, Umeyama T, Wang CC (2009). The Aurora Kinase in Trypanosoma brucei plays distinctive roles in metaphase-anaphase transition and cytokinetic initiation. PLoS Pathog 5, e1000575.
Li Z, Wang CC (2008). KMP-11, a basal body and flagellar protein, is required for cell division in Trypanosoma brucei. Eukaryotic Cell 7, 1941–1950.
Lowery DM, Clauser KR, Hjerrild M, Lim D, Alexander J, Kishi K, Ong S-E, Gammeltoft S, Carr SA, Yaffe MB (2007). Proteomic screen defines the Polo-box domain interactome and identifies Rock2 as a Plk1 substrate. EMBO J 26, 2262–2273.
Lozano-Núñez A, Ikeda KN, Sauer T, de Graffenried CL (2013). An analogue-sensitive approach identifies basal body rotation and flagellum attachment zone elongation as key functions of PLK in Trypanosoma brucei. Mol Biol Cell 24, 1321–1333.
MacGregor P, Savill NJ, Hall D, Matthews KR (2011). Transmission stages dominate trypanosome within-host dynamics during chronic infections. Cell Host Microbe 9, 310–318.
Matthews KR, Gull K (1994). Evidence for an interplay between cell cycle progression and the initiation of differentiation between life cycle forms of African trypanosomes. J Cell Biol 125, 1147–1156.
McKean PG (2003). Coordination of cell cycle and cytokinesis in Trypanosoma brucei. Curr Opin Microbiol 6, 600–607.
Moreira-Leite FF, Sherwin T, Kohl L, Gull K (2001). A trypanosome structure involved in transmitting cytoplasmic information during cell division. Science 294, 610–612.
Morriswood B, Havlicek K, Demmel L, Yavuz S, Sealey-Cardona M, Vidilaseris K, Anrather D, Kostan J, Djinovic-Carugo K, Roux KJ, *et al.* (2013). Novel bilobe components in Trypanosoma brucei identified using proximity-dependent biotinylation. Eukaryot Cell 12, 356–367.
Morriswood B, He CY, Sealey-Cardona M, Yelinek J, Pypaert M, Warren G (2009). The bilobe structure of Trypanosoma brucei contains a MORN-repeat protein. Mol Biochem Parasitol 167, 95–103.
Mott GA, Wilson R, Fernando A, Robinson A, MacGregor P, Kennedy D, Schaap D, Matthews JB, Matthews KR (2011). Targeting cattle-borne zoonoses and cattle pathogens using a novel trypanosomatid-based delivery system. PLoS Pathog 7, e1002340.
Murugan RN, Park J-E, Kim E-H, Shin SY, Cheong C, Lee KS, Bang JK (2011). Plk1-targeted small molecule inhibitors: molecular basis for their potency and specificity. Mol Cells 32, 209–220.
Obado SO, Rout MP (2012). Ciliary and nuclear transport: different places, similar routes? Dev Cell 22, 693–694.
Park S-H, Zarrinpar A, Lim WA (2003). Rewiring MAP kinase pathways using alternative scaffold assembly mechanisms. Science 299, 1061–1064.
Pays E, Vanhollebeke B (2009). Human innate immunity against African trypanosomes. Curr Opin Immunol 21, 493–498.
Peifer M, Berg S, Reynolds AB (1994). A repeating amino acid motif shared by proteins with diverse cellular roles. Cell 76, 789–791.
Ploubidou A, Robinson DR, Docherty RC, Ogbadoyi EO, Gull K (1999). Evidence for novel cell cycle checkpoints in trypanosomes: kinetoplast segregation and cytokinesis in the absence of mitosis. J Cell Sci 112, 4641–4650.
Pradel LC, Bonhivers M, Landrein N, Robinson DR (2006). NIMA-related kinase TbNRKC is involved in basal body separation in Trypanosoma brucei. J Cell Sci 119, 1852–1863.
Robinson DR, Gull K (1991). Basal body movements as a mechanism for mitochondrial genome segregation in the trypanosome cell cycle. Nature 352, 731–733.
Rotureau B, Subota I, Buisson J, Bastin P (2012). A new asymmetric division contributes to the continuous production of infective trypanosomes in the tsetse fly. Development 139, 1842–1850.
Roux KJ, Kim DI, Raida M, Burke B (2012). A promiscuous biotin ligase fusion protein identifies proximal and interacting proteins in mammalian cells. J Cell Biol 196, 801–810.
Schneider A, Hemphill A, Wyler T, Seebeck T (1988). Large microtubule-associated protein of T. brucei has tandemly repeated, near-identical sequences. Science 241, 459–462.
Schneider A, Plessmann U, Weber K (1997). Subpellicular and flagellar microtubules of Trypanosoma brucei are extensively glutamylated. J Cell Sci 110, 431–437.
Sharma R, Peacock L, Gluenz E, Gull K, Gibson W, Carrington M (2008). Asymmetric cell division as a route to reduction in cell length and change in cell morphology in trypanosomes. Protist 159, 137–151.
Sherwin T, Gull K (1989). The cell division cycle of Trypanosoma brucei brucei: timing of event markers and cytoskeletal modulations. Philos Trans R Soc Lond B Biol Sci 323, 573–588.
Snead JL, Sullivan M, Lowery DM, Cohen MS, Zhang C, Randle DH, Taunton J, Yaffe MB, Morgan DO, Shokat KM (2007). A coupled chemical-genetic and bioinformatic approach to Polo-like kinase pathway exploration. Chem Biol 14, 1261–1272.
Steinert PM, Kartasova T, Marekov LN (1998). Biochemical evidence that small proline-rich proteins and trichohyalin function in epithelia by modulation of the biomechanical properties of their cornified cell envelopes. J Biol Chem 273, 11758–11769.
Steinert PM, Parry DAD, Marekov LN (2003). Trichohyalin mechanically strengthens the hair follicle: multiple cross-bridging roles in the inner root sheath. J Biol Chem 278, 41409–41419.
Sunter JD, Varga V, Dean S, Gull K (2015). A dynamic coordination of flagellum and cytoplasmic cytoskeleton assembly specifies cell morphogenesis in trypanosomes. J Cell Sci 128, 1580–1594.
Taylor AER, Godfrey DG (1969). A new organelle of bloodstream salivarian trypanosomes. J Protozool 16, 466–470.
Tu X, Wang CC (2004). The involvement of two cdc2-related kinases (CRKs) in Trypanosoma brucei cell cycle regulation and the distinctive stage-specific phenotypes caused by CRK3 depletion. J Biol Chem 279, 20519–20528.
Urbaniak MD, Guther MLS, Ferguson MAJ (2012). Comparative SILAC proteomic analysis of Trypanosoma brucei bloodstream and procyclic lifecycle stages. PLoS One 7, e36619.
Urbaniak MD, Martin DMA, Ferguson MAJ (2013). Global quantitative SILAC phosphoproteomics reveals differential phosphorylation is widespread between the procyclic and bloodstream form lifecycle stages of Trypanosoma brucei. J Proteome Res 12, 2233–2244.
Vaughan S (2010). Assembly of the flagellum and its role in cell morphogenesis in Trypanosoma brucei. Curr Opin Microbiol 13, 453–458.
Vaughan S, Kohl L, Ngai I, Wheeler RJ, Gull K (2008). A repetitive protein essential for the flagellum attachment zone filament structure and function in Trypanosoma brucei. Protist 159, 127–136.
Vickerman K (1969). On the surface coat and flagellar adhesion in trypanosomes. J Cell Sci 5, 163–193.
Welburn SC, Maudlin I (2012). Priorities for the elimination of sleeping sickness. Adv Parasitol 79, 299–337.
Wirtz E, Leal S, Ochatt C, Cross GA (1999). A tightly regulated inducible expression system for conditional gene knock-outs and dominant-negative genetics in Trypanosoma brucei. Mol Biochem Parasitol 99, 89–101.
Wiśniewski JR, Zougman A, Nagaraj N, Mann M (2009). Universal sample preparation method for proteome analysis. Nat Methods 6, 359–362.
Yu Z, Liu Y, Li Z (2012). Structure-function relationship of the Polo-like kinase in Trypanosoma brucei. J Cell Sci 125, 1519–1530.
Yun S-M, Moulaei T, Lim D, Bang JK, Park JE, Shenoy SR, Liu F, Kang YH, Liao C, Soung NK, *et al.* (2009). Structural and functional analyses of minimal phosphopeptides targeting the polo-box domain of polo-like kinase 1. Nat Struct Mol Biol 16, 876–882.
Zhou Q, Gheiratmand L, Chen Y, Lim TK, Zhang J, Li S, Xia N, Liu B, Lin Q, He CY (2010). A comparative proteomic analysis reveals a new bi-lobe protein required for bi-lobe duplication and cell division in Trypanosoma brucei. PLoS One 5, e9660.
Zhou Q, Liu B, Sun Y, He CY (2011). A coiled-coil- and C2-domain-containing protein is required for FAZ assembly and cell morphology in Trypanosoma brucei. J Cell Sci 124, 3848–3858.
Zitouni S, Nabais C, Jana SC, Guerrero A, Bettencourt-Dias M (2014). Polo-like kinases: structural variations lead to multiple functions. Nat Rev Mol Cell Biol 15, 433–452.